

A polynomial-based constrained solver for fuel-optimal low-thrust trajectory optimization

Thomas Caleb *

ISAE-SUPAERO, 31055, Toulouse, France

Roberto Armellin †

University of Auckland, Auckland, 1142, New Zealand

Spencer Boone ‡ and Stéphanie Lizy-Destrez §

ISAE-SUPAERO, 31055, Toulouse, France

Differential dynamic programming (DDP) is a trajectory optimization method, particularly resilient to poor initial guesses. However, its long run times compared to other methods make it less suitable for embedded systems. In this work, we introduce polynomial-based DDP methods capable of enforcing constraints while optimizing for fuel efficiency. Additionally, a polynomial-based Newton solver is implemented to enforce constraints with high precision. The proposed solver, differential algebra-based differential dynamic programming (DADDy), is validated and tested on various astrodynamics scenarios. Results demonstrate that DADDy achieves the same solutions as state-of-the-art DDP methods but with significantly reduced run times. Specifically, for the scenarios investigated in this work, the most stable method was able to achieve 100% convergence and achieved runtime reductions of 70% in the Sun-centered two-body problem, 23% to 94% in the Earth-Moon CR3BP, and 46% to 59% in the Earth-centered two-body problem.

I. Introduction

Newly developed space missions aim to explore complex environments with nonlinear dynamics, such as the Earth-Moon system [1, 2]. However, optimization solvers may struggle in these regimes, being both time-consuming and highly sensitive to parameter settings [3]. Furthermore, as many new missions aim to achieve autonomy, onboard trajectory adjustments and computations become essential [4]. Current nonlinear trajectory optimization solvers are computationally intensive, making them unsuitable for satellites with limited onboard processing power. While faster methods exist, they typically rely on linear approximations of the dynamics, which can be inaccurate [5]. This work

*Ph.D. applicant, DCAS/SaCLaB, thomas.caleb@isae-supero.fr

†Full Professor, Te Pūnaha Ōtea – Space Institute, roberto.armellin@auckland.ac.nz

‡Post-doctoral fellow, DCAS/SaCLaB, spencer.boone@isae-supero.fr

§Full Professor, DCAS/SaCLaB, stephanie.lizy-destrez@isae-supero.fr

presents a method for accurate and efficient constrained nonlinear trajectory optimization, addressing these limitations and advancing the potential for autonomous space missions.

Differential dynamic programming (DDP) is a trajectory optimization method developed by Mayne [6] and used in mission analysis in the NASA missions Dawn [7] and Psyche [8]. It has the advantage of being robust to poor first guesses and adaptable to various optimization problems. Many extensions of the original framework followed [9–12]. The method of Howell et al. [13] add constraint management using an augmented Lagrangian (AUL) formulation, followed by a so-called "solution polishing" using a Newton method to obtain a solution feasible at a high precision. Boone and McMahon [14] leverage high-order Taylor polynomials [15, 16] to approximate the nonlinear dynamics and lower the computation burden of DDP. This method requires an initial trajectory in the neighborhood of the optimal solution and can easily be embedded in case of trajectory modification or to account for navigation errors.

The authors introduce a method to accelerate constrained DDP using high-order Taylor expansion for automatic differentiation and dynamics approximation without requiring an initial feasible trajectory. Additionally, the work present a method for performing fuel-optimal trajectory optimization. High-order Taylor expansions are further employed to expedite the solution polishing phase.

After introducing DDP, AUL formulation, and high-order Taylor polynomials in Section II, Section III details the proposed methodology. Section IV applies these methods to various test cases from the literature to validate and compare them with the state of the art. Finally, Section V presents the conclusions.

II. Background

A. Constrained differential dynamic programming

1. Differential dynamic programming

DDP tackles optimization problems of N stages with dynamics of type: $\mathbf{x}_{k+1} = \mathbf{f}(\mathbf{x}_k, \mathbf{u}_k)$ [6, 9], where $k \in [0, N - 1]$, $\mathbf{x}_k \in \mathbb{R}^{N_x}$ is the state vector, $\mathbf{u}_k \in \mathbb{R}^{N_u}$ is the control, \mathbf{f} is the dynamics. The initial and target state vectors \mathbf{x}_0 and \mathbf{x}_t of size N_x are given, and the cost function to minimize is:

$$J(\mathbf{U}) = \sum_{i=0}^{N-1} l(\mathbf{x}_i, \mathbf{u}_i) + \Phi(\mathbf{x}_N, \mathbf{x}_t) \quad (1)$$

where $\mathbf{U} = (\mathbf{u}_0, \mathbf{u}_1, \dots, \mathbf{u}_{N-1})$ is the vector of controls of size $N \cdot N_u$, \mathbf{x}_N is the final propagated state vector, l is the stage cost, and Φ is the terminal cost.

Let us define some notations: (1) A subscript k is used to indicate that dynamics, constraints, or cost functions are

evaluated at the step k , for instance $f_k = f(\mathbf{x}_k, \mathbf{u}_k)$ and $\Phi_k = \Phi(\mathbf{x}_k, \mathbf{x}_t)$. (2) Partial derivatives of a function h with respect to a given variable y are written as: $h_y = \frac{\partial h}{\partial y}$. Second order derivatives with respect to y then z : $\frac{\partial^2 h}{\partial z \partial y}$, are written h_{yz} . (3) A comma between subscripts indicates the step, and then the derivative index: $\frac{\partial^2 f}{\partial x^2}(\mathbf{x}_k, \mathbf{u}_k) = f_{k,xx}$. (4) The i -th component of a vector \mathbf{y} is written y^i , and the term at the i -th row and j -th column of a matrix \mathbf{y} is written $y^{i,j}$. Let $\mathbf{X} = (\mathbf{x}_0, \mathbf{x}_1, \dots, \mathbf{x}_N)$ and V_k , the minimized cost-to-go:

$$V_k(\mathbf{x}_k) = \min_{\mathbf{U}_k} \left[\sum_{i=k}^{N-1} l(\mathbf{x}_i, \mathbf{u}_i) + \Phi(\mathbf{x}_N, \mathbf{x}_t) \right] \quad (2)$$

where $\mathbf{U}_k = (\mathbf{u}_k, \mathbf{u}_{k+1}, \dots, \mathbf{u}_{N-1})$. Note that $V_0 = \min_{\mathbf{U}} J$. Then, following Bellman's principle of optimality: $V_k(\mathbf{x}_k) = \min_{\mathbf{u}_k} [l(\mathbf{x}_k, \mathbf{u}_k) + V_{k+1}(\mathbf{x}_{k+1})] = \min_{\mathbf{u}_k} [l(\mathbf{x}_k, \mathbf{u}_k) + V_{k+1}(f(\mathbf{x}_k, \mathbf{u}_k))]$. Therefore, the cost-to-go at stage k is defined as: $Q_k(\mathbf{x}_k, \mathbf{u}_k) = l(\mathbf{x}_k, \mathbf{u}_k) + V_{k+1}(f(\mathbf{x}_k, \mathbf{u}_k))$.

The partial derivatives of the cost-to-go are computed as:

$$\begin{cases} Q_{k,x} &= l_x + V_{k+1,x} \cdot f_{k,x} \\ Q_{k,u} &= l_u + V_{k+1,x} \cdot f_{k,u} \\ Q_{k,xx} &= l_{k,xx} + f_{k,x}^T \cdot V_{k+1,xx} \cdot f_{k,x} \left(+ \sum_{i=1}^{N_x} V_{k+1,x}^i \cdot (f_k^i)_{xx} \right) \\ Q_{k,xu} &= l_{k,xu} + f_{k,x}^T \cdot V_{k+1,xx} \cdot f_{k,u} \left(+ \sum_{i=1}^{N_x} V_{k+1,x}^i \cdot (f_k^i)_{xu} \right) \\ Q_{k,uu} &= l_{k,uu} + f_{k,u}^T \cdot V_{k+1,xx} \cdot f_{k,u} \left(+ \sum_{i=1}^{N_x} V_{k+1,x}^i \cdot (f_k^i)_{uu} \right) \end{cases} \quad (3)$$

where the terms between the parentheses are not taken into account in several DDP algorithms [6, 13]. They account for the second-order derivatives of the dynamics. These computations are initialized with $V_{N,x} = \Phi_x$ and $V_{N,xx} = \Phi_{xx}$.

The DDP algorithm consists in two phases. The first phase is the backward sweep and consists in finding the control correction that minimizes the cost-to-go Q_k at each step. The latter is approximated by a quadratic function using Eq. (3). Given \mathbf{X} and \mathbf{U} , it computes the control law corrections $\mathbf{A} = (\mathbf{a}_0, \mathbf{a}_1, \dots, \mathbf{a}_{N-1})$, and $\mathbf{B} = (\mathbf{b}_0, \mathbf{b}_1, \dots, \mathbf{b}_{N-1})$ starting from $k = N - 1$ to $k = 0$, with:

$$\begin{cases} \mathbf{a}_k &= -\mathbf{Q}_{k,uu}^{-1} \cdot \mathbf{Q}_{k,u} \\ \mathbf{b}_k &= -\mathbf{Q}_{k,uu}^{-1} \cdot \mathbf{Q}_{k,xu}^T \\ V_{k,x} &= Q_{k,x} + Q_{k,xu} \cdot \mathbf{a}_k \\ V_{k,xx} &= Q_{k,xx} + Q_{k,xu} \cdot \mathbf{b}_k \end{cases} \quad (4)$$

The backward sweep is presented in Alg. 1. The second phase is the forward pass. It updates \mathbf{X} and \mathbf{U} considering the

Algorithm 1 Backward sweep

Input: X, U, x_t, f, l, Φ
 $k \leftarrow N - 1$
Compute $V_{N,x}$ and $V_{N,xx}$
while $k \geq 0$ **do**
 Compute $f_{k,x}, f_{k,u}$
 Compute $l_{k,x}, l_{k,u}, l_{k,xx}, l_{k,xu}, l_{k,uu}$
 Compute $Q_{k,x}, Q_{k,u}, Q_{k,xx}, Q_{k,xu}, Q_{k,uu}$
 $a_k, b_k \leftarrow -Q_{k,uu}^{-1} \cdot Q_{k,u}^T, -Q_{k,uu}^{-1} \cdot Q_{k,xu}^T$
 Compute $V_{k,x}$ and $V_{k,xx}$
 $k \leftarrow k - 1$
end while
Return: A, B

control law corrections A and B starting from $k = 0$ to $k = N - 1$. The new states are x_k^* and the new controls are u_k^* . Note that $x_0^* = x_0$. They are retrieved iteratively:

$$\begin{cases} \delta x_k^* &= x_k^* - x_k \\ u_k^* &= u_k + \delta u_k^* = u_k + a_k + b_k \cdot \delta x_k^* \\ x_{k+1}^* &= f(x_k^*, u_k^*) \end{cases} \quad (5)$$

The forward pass execution is shown in Alg. 2, and the full DDP process is presented in Alg. 3, where ε_{DDP} is the tolerance of the method.

Algorithm 2 Forward pass

Input: $X, U, x_t, A, B, f, l, \Phi$
 $k \leftarrow 0$
 $J^*, x_0^* \leftarrow 0, x_0$
while $k \leq N - 1$ **do**
 $\delta x_k^* \leftarrow x_k^* - x_k$
 $u_k^* \leftarrow u_k + a_k + b_k \cdot \delta x_k^*$
 $x_{k+1}^* \leftarrow f(x_k^*, u_k^*)$
 $J^* \leftarrow J^* + l(x_k^*, u_k^*)$
 $k \leftarrow k + 1$
end while
 $J^* \leftarrow J^* + \Phi(x_N^*, x_t)$
Return: J^*, X^*, U^*

Algorithm 3 DDP solver

Input: $\varepsilon_{\text{DDP}}, \mathbf{x}_0, \mathbf{x}_t, \mathbf{U}_0, \mathbf{f}, l, \Phi$

$J, \mathbf{U} \leftarrow -\infty, \mathbf{U}_0$

Compute X and J^*

while $J^* < J \wedge |J - J^*| > \varepsilon_{\text{DDP}}$ **do**

$J \leftarrow J^*$

$\mathbf{A}, \mathbf{B} \leftarrow \text{BackwardSweep}(X, \mathbf{U}, \mathbf{x}_t, \mathbf{f}, l, \Phi)$

$J^*, X^*, \mathbf{U}^* \leftarrow \text{ForwardPass}(X, \mathbf{U}, \mathbf{x}_t, \mathbf{A}, \mathbf{B}, \mathbf{f}, l, \Phi)$

$X, \mathbf{U} \leftarrow X^*, \mathbf{U}^*$

end while

Return: J^*, X, \mathbf{U}

2. Augmented Lagrangian formulation

DDP as presented by Mayne [6] does not implement constraints. This work implements them following the work of Howell et al. [13]. They can tackle path constraints:

$$\begin{cases} \mathbf{g}_{ineq}(\mathbf{x}_k, \mathbf{u}_k) \leq \mathbf{0} \\ \mathbf{g}_{eq}(\mathbf{x}_k, \mathbf{u}_k) = \mathbf{0} \end{cases} \quad (6)$$

where \mathbf{g}_{ineq} are the inequality path constraints of size N_{ineq} , and \mathbf{g}_{eq} are the equality path constraints of size N_{eq} . They also implement terminal constraints:

$$\begin{cases} \mathbf{g}_{tineq}(\mathbf{x}_N, \mathbf{x}_t) \leq \mathbf{0} \\ \mathbf{g}_{teq}(\mathbf{x}_N, \mathbf{x}_t) = \mathbf{0} \end{cases} \quad (7)$$

where \mathbf{g}_{tineq} are the terminal inequality constraints of size N_{tineq} , and \mathbf{g}_{teq} are the terminal equality constraints of size N_{teq} . Let us define: $\mathbf{g} = [\mathbf{g}_{ineq}^T, \mathbf{g}_{eq}^T]^T$, $\mathbf{g}_t = [\mathbf{g}_{tineq}^T, \mathbf{g}_{teq}^T]^T$, and $\mathbf{g}_N = [\mathbf{g}_{tineq}(\mathbf{x}_N, \mathbf{x}_t)^T, \mathbf{g}_{teq}(\mathbf{x}_N, \mathbf{x}_t)^T] = \mathbf{g}_t(\mathbf{x}_N, \mathbf{x}_t)$. These constraints are handled using the AUL formulation. It consists in augmenting the cost function with the constraints. The DDP solver will then minimize the cost, thus, it will satisfy the constraints:

$$\begin{cases} \tilde{l}(\mathbf{x}_k, \mathbf{u}_k, \lambda_k, \mu_k) = l_k + \left[\lambda_k + \frac{\mathcal{I}_{\mu,k}}{2} \cdot \mathbf{g}_k \right]^T \cdot \mathbf{g}_k \\ \tilde{\Phi}(\mathbf{x}_N, \mathbf{x}_t, \lambda_N, \mu_N) = \Phi_N + \left[\lambda_N + \frac{\mathcal{I}_{\mu,N}}{2} \cdot \mathbf{g}_N \right]^T \cdot \mathbf{g}_N \end{cases} \quad (8)$$

where the tilde denotes augmented cost functions, λ_k is the dual state of size $N_{ineq} + N_{eq}$ if $k \in [0, N - 1]$ or of size $N_{tineq} + N_{teq}$ if $k = N$, where μ_k is the penalty vector of same size as λ_k . $\mathcal{I}_{\mu,k}$ is a diagonal matrix of the same size as λ_k , its i -th diagonal term is 0 if g_k^i is an inequality, $g_k^i < 0$, and $\lambda_k^i = 0$, or μ_k^i otherwise. The dual states and penalty

vectors are updated at each AUL solving round as:

$$\left\{ \begin{array}{l} (\lambda_k^i)^* = \max\left(0, \lambda_k^i + \mu_k^i \cdot g_{ineq}^i(\mathbf{x}_k^*, \mathbf{u}_k^*)\right), \text{ if } k \in [0, N-1] \wedge i \in [1, N_{ineq}] \\ (\lambda_k^i)^* = \lambda_k^i + \mu_k^i \cdot g_{eq}^{i-N_{ineq}}(\mathbf{x}_k^*, \mathbf{u}_k^*), \text{ if } k \in [0, N-1] \wedge i \in [1 + N_{ineq}, N_{ineq} + N_{eq}] \\ (\lambda_N^i)^* = \max\left(0, \lambda_N^i + \mu_N^i \cdot g_{ineq}^i(\mathbf{x}_N^*, \mathbf{x}_t)\right), \text{ if } i \in [1, N_{tineq}] \\ (\lambda_N^i)^* = \lambda_N^i + \mu_N^i \cdot g_{teq}^{i-N_{tineq}}(\mathbf{x}_N^*, \mathbf{x}_t), \text{ if } i \in [1 + N_{tineq}, N_{tineq} + N_{teq}] \\ \mu_k^* = \gamma \cdot \mu_k \end{array} \right. \quad (9)$$

where $\gamma > 1$ is the penalty growth rate. Let us define $\Lambda = (\lambda_0, \lambda_1, \dots, \lambda_N)$, $\mathbf{M} = (\mu_0, \mu_1, \dots, \mu_N)$, and $\mathbf{G} = (g_0, g_1, \dots, g_N)$. The augmented problem is solved using DDP until the maximum constraints violation g_{\max} is below the target constraint satisfaction $\varepsilon_{\text{AUL}} > 0$, as shown in Alg. 4.

Algorithm 4 AUL solver

Input: $\varepsilon_{\text{DDP}}, \varepsilon_{\text{AUL}}, \mathbf{x}_0, \mathbf{x}_t, U_0, f, l, \Phi, \mathbf{g}, \mathbf{g}_t$
 $U \leftarrow U_0$
Initialize Λ and \mathbf{M}
Compute \mathbf{X}, \mathbf{G} , and g_{\max}
while $g_{\max} > \varepsilon_{\text{AUL}}$ **do**
 Compute \tilde{l} and $\tilde{\Phi}$
 $J, \mathbf{X}, U \leftarrow \text{DDP}(\varepsilon_{\text{DDP}}, \mathbf{x}_0, \mathbf{x}_t, U, f, \tilde{l}, \tilde{\Phi})$
 Compute \mathbf{G}
 Update Λ and \mathbf{M}
 $g_{\max} \leftarrow \max \mathbf{G}$
end while
Return: $J, \mathbf{X}, U, g_{\max}$

B. Solution polishing using a projected Newton method

In Howell et al. [13], the authors show how stopping the AUL solver at a low accuracy ε_{AUL} to then perform solution polishing to satisfy the constraints with high precision $\varepsilon_N < \varepsilon_{\text{AUL}}$, using a Newton method, can prove significantly faster than converging to this precision using the AUL solver. It consists in concatenating all the active constraints in a single vector Γ of size $N_\Gamma \leq N \cdot (N_{ineq} + N_{eq} + N_x) + N_{tineq} + N_{teq}$, including continuity equality constraints: $\mathbf{h}_k = \mathbf{h}(\mathbf{x}_k, \mathbf{u}_k, \mathbf{x}_{k+1}) = \mathbf{x}_{k+1} - \mathbf{f}(\mathbf{x}_k, \mathbf{u}_k) = \mathbf{0}$. The controls and the state vectors that can be modified, i.e., all of them except \mathbf{x}_0 , are concatenated in a vector $\mathbf{Y} = [\mathbf{u}_0^T, \mathbf{x}_1^T, \mathbf{u}_0^T, \dots, \mathbf{x}_{N-1}^T, \mathbf{u}_{N-1}^T, \mathbf{x}_N^T]^T$ of size $N_Y = N \cdot (N_x + N_u)$. The active constraints are linearized: $\Gamma(\mathbf{Y}) \approx \Delta \cdot \delta\mathbf{Y} + \mathbf{d}$, with Δ and \mathbf{d} respectively the constraints gradient and values at \mathbf{Y} , and $\delta\mathbf{Y}$ is a small variation around \mathbf{Y} . The correction $\delta\mathbf{Y}^* = -\Delta \backslash \mathbf{d}$ provides a refined \mathbf{Y}^* . It is the solution to the non-square system: $\Delta \cdot \mathbf{z} = -\mathbf{d}$ of unknown \mathbf{z} . The entire process is presented in Alg. 5. The parameter ε_{CV} is typically set to 1.1. The result is an solution that satisfies the optimality criterion to tolerance ε_{DDP} , while satisfying the constraints to the

Algorithm 5 Newton solver

Input: $\varepsilon_N, X_0, U_0, \mathbf{x}_t, \mathbf{f}, \mathbf{g}, \mathbf{g}_t$

$\gamma, d_{\max} \leftarrow 0.5, +\infty$

Compute Y

Retrieve d

while $d_{\max} > \varepsilon_N$ **do**

 Compute Δ at Y

$r \leftarrow +\infty$

while $d_{\max} > \varepsilon_N \wedge r > \varepsilon_{CV}$ **do**

 ▸ Reuse Δ

$d_{\max}^*, \alpha \leftarrow +\infty, 1$

while $d_{\max}^* > d_{\max}$ **do**

 ▸ Linesearch

$Y^* \leftarrow Y - \alpha \cdot \Delta \setminus d$

$d^* \leftarrow \Gamma(Y^*)$

$d_{\max}^*, \alpha \leftarrow \max |d^*|, \gamma \cdot \alpha$

end while

$r, d_{\max} \leftarrow \log d_{\max}^* / \log d_{\max}, d_{\max}^*$

$d, Y \leftarrow d^*, Y^*$

end while

end while

Return: X, U, d_{\max}

tolerance ε_N .

C. Differential Algebra

Differential algebra (DA) is the dedicated framework to manipulate high-order Taylor expansions [15]. It consists of assimilating a given sufficiently differentiable function \mathbf{h} of ν variables, with its Taylor expansion \mathcal{P}_h . It provides a description of \mathbf{h} over its domain. Furthermore, algebraic and functional operations, including polynomial inversion, are well-defined on the set of all Taylor polynomials [17].

The DA framework provides automatic differentiation. Indeed, the variable is defined as a vector of polynomials: $\mathcal{P}_\nu = \nu + \delta\nu$. Where ν is the constant part and $\delta\nu$ is a perturbation vector. Evaluating a function \mathbf{h} at point \mathcal{P}_ν returns a Taylor expansion \mathcal{P}_h of \mathbf{h} around ν . The derivatives of \mathbf{h} at ν can be retrieved effortlessly in the coefficients of \mathcal{P}_h . Moreover, given a Taylor expansion \mathcal{P}_h of \mathbf{h} around point ν , for all $\varepsilon > 0$, there is a $R_\varepsilon > 0$ such that [18]:

$$\|\delta\nu\|_2 \leq R_\varepsilon \implies \|\mathcal{P}_h(\delta\nu) - \mathbf{h}(\nu + \delta\nu)\|_2 \leq \varepsilon \quad (10)$$

in other words, \mathcal{P}_h is a local approximation of \mathbf{h} around the point ν . This feature proves useful when evaluations of the function h are costly. Thus, such an approximation greatly reduces run time [16].

Throughout the paper, the constant part of a polynomial \mathcal{P}_h is denoted $\overline{\mathcal{P}_h}$, a small, unset, perturbation of any given quantity y is denoted δy , and the value R_ε is called the convergence radius of \mathcal{P}_h at accuracy ε .

III. Methodology

This section first tackles using high-order Taylor polynomials in DDP in the differential algebra-based differential dynamic programming (DADDy) solver. Then, a method to perform fuel-optimal optimization is shown, followed by an enhanced solution polishing method.

A. DA-based DDP

1. Automatic differentiation

Automatic differentiation is implemented using the DA framework. States and controls are defined as vectors of polynomials: $\mathcal{P}_x = \mathbf{x} + \delta\mathbf{x}$ and $\mathcal{P}_u = \mathbf{u} + \delta\mathbf{u}$, where \mathbf{x} (respectively \mathbf{u}) is a computed state vector (control) and $\delta\mathbf{x}$ ($\delta\mathbf{u}$) is a perturbation vector of size N_x (N_u). Therefore, evaluating any function \mathbf{h} at point $(\mathcal{P}_x, \mathcal{P}_u)$ at order 2 returns a second-order Taylor expansion \mathcal{P}_h of \mathbf{h} at (\mathbf{x}, \mathbf{u}) . Then, its first-order derivatives \mathbf{h}_x and \mathbf{h}_u , and second-order derivatives \mathbf{h}_{xx} , \mathbf{h}_{xu} , and \mathbf{h}_{uu} are retrieved in the coefficients of \mathcal{P}_h . Thus, the derivatives of f , \tilde{l} , and $\tilde{\Phi}$ can be retrieved without implementing the derivatives by hand [9] or being limited to linear and quadratic problems [13]. The previous considerations result in a polynomial-based forward pass, shown in Alg. 6. It allows for automatic differentiation of the dynamics, stage cost, and terminal cost functions, as they are evaluated using the DA variables $\delta\mathbf{x}$, and $\delta\mathbf{u}$. For short, the following notation is used: $\mathcal{P}_l = (\mathcal{P}_{l,0}, \mathcal{P}_{l,1}, \dots, \mathcal{P}_{l,N-1})$, similarly for \mathcal{P}_f . Consequently, a novel backward sweep

Algorithm 6 Forward pass with automatic differentiation

Input: $X, U, \mathbf{x}_t, A, B, f, l, \Phi$
 $k \leftarrow 0$
 $J^*, \mathbf{x}_k^* \leftarrow 0, \mathbf{x}_0$
while $k \leq N - 1$ **do**
 $\delta\mathbf{x}_k^* \leftarrow \mathbf{x}_k^* - \mathbf{x}_k$
 $\mathbf{u}_k^* \leftarrow \mathbf{u}_k + \mathbf{a}_k + \mathbf{b}_k \cdot \delta\mathbf{x}_k^*$
 $\mathcal{P}_{f,k}, \mathcal{P}_{l,k} \leftarrow f(\mathbf{x}_k^* + \delta\mathbf{x}, \mathbf{u}_k^* + \delta\mathbf{u}), l(\mathbf{x}_k^* + \delta\mathbf{x}, \mathbf{u}_k^* + \delta\mathbf{u})$
 $\mathbf{x}_{k+1}^*, J^* \leftarrow \overline{\mathcal{P}_{f,k}}, J^* + \overline{\mathcal{P}_{l,k}}$
 $k \leftarrow k + 1$
end while
 $\mathcal{P}_\Phi \leftarrow \Phi(\mathbf{x}_N^* + \delta\mathbf{x}, \mathbf{x}_t)$
 $J^* \leftarrow J^* + \overline{\mathcal{P}_\Phi}$
Return: $J^*, \mathbf{X}^*, U^*, \mathcal{P}_f, \mathcal{P}_l, \mathcal{P}_\Phi$

using the automatic differentiation of Alg. 6 is shown in Alg. 7.

2. Enhanced forward pass: Approximation of the dynamics

Boone and McMahon [14] highlight that the forward pass is one order of magnitude slower than the backward sweep due to dynamics evaluation. It is the reason why they use DA (or state transition tensors (STTs)) to accelerate optimization, given an initial trajectory. In this work, this principle is applied at every iteration of DDP to accelerate the evaluation of the dynamics. The polynomial expansion of the dynamics $\mathcal{P}_{f,k}(\delta\mathbf{x}, \delta\mathbf{u})$ at stage k is already computed for the

Algorithm 7 Backward sweep with automatic differentiation

Input: $X, U, x_t, \mathcal{P}_f, \mathcal{P}_l, \mathcal{P}_\Phi$
 Retrieve $V_{N,x}$ and $V_{N,xx}$ from \mathcal{P}_Φ
 $k \leftarrow N - 1$
while $k \geq 0$ **do**
 Retrieve $f_{k,x}, f_{k,u}$ from $\mathcal{P}_{f,k}$
 Retrieve $l_{k,x}, l_{k,u}, l_{k,xx}, l_{k,xu}, l_{k,uu}$ from $\mathcal{P}_{l,k}$
 Compute $Q_{k,x}, Q_{k,u}, Q_{k,xx}, Q_{k,xu}, Q_{k,uu}$
 $a_k, b_k \leftarrow -Q_{k,uu}^{-1} \cdot Q_{k,u}^T, -Q_{k,uu}^{-1} \cdot Q_{k,xu}^T$
 Compute $V_{k,x}$ and $V_{k,xx}$
 $k \leftarrow k - 1$
end while
Return: A, B

automatic differentiation and can be leveraged to avoid recomputing the dynamics when the corrections $(\delta x_k^*, \delta u_k^*)$ computed in Eq. (5) are small. They need to be within the convergence radius $R_{\mathcal{P}_{f,k}, \varepsilon_{\text{DA}}}$ of $\mathcal{P}_{f,k}$, defined in Eq. (10), where the accuracy is $\varepsilon_{\text{DA}} > 0$ and $\|\delta v\|_2 = \sqrt{\|\delta x_k^*\|_2^2 + \|\delta u_k^*\|_2^2}$. Finally, the dynamics are now evaluated as:

$$\begin{cases}
 \mathbf{x}_{k+1}^* & \approx \mathcal{P}_{f,k}(\delta \mathbf{x}_k^*, \delta \mathbf{u}_k^*), \text{ if } \sqrt{\|\delta \mathbf{x}_k^*\|_2^2 + \|\delta \mathbf{u}_k^*\|_2^2} \leq R_{\mathcal{P}_{f,k}, \varepsilon_{\text{DA}}} \\
 \mathbf{x}_{k+1}^* & = \overline{f(\mathcal{P}_{x_k^*}, \mathcal{P}_{u_k^*})}, \text{ otherwise}
 \end{cases} \quad (11)$$

Note that the second case leads to recomputing the dynamics and their Taylor expansions, while the first case only consists in performing N_x polynomial compositions of $N_x + N_u$ variables to obtain the dynamics and their associated derivatives. This approach leads to the novel polynomial-based forward pass of Alg. 8. It also allows for automatic differentiation and implements polynomial approximation of the dynamics using the already computed polynomial representations of f .

3. Enhanced Backward sweeps: cost-to-go derivatives computations

In most DDP solvers, the derivatives of the cost-to-go Q_k given in Eq. (3) do not include the second-order derivatives of the dynamics. These derivatives will already be computed for the dynamics approximation and can be added without requiring additional computations or numerical integrations. Consequently, the authors introduce a novel backward sweep method that implements dynamics Hessians and automatic differentiation, shown in Alg. 9.

Moreover, Q_k can be directly evaluated as $\mathcal{P}_{Q,k} = l(\mathcal{P}_{x,k}, \mathcal{P}_{u,k}) + V_{k+1}(f(\mathcal{P}_{x,k}, \mathcal{P}_{u,k}))$. The partial derivatives of Q_k can then be retrieved from the coefficients to avoid matrix computations. Note that the second-order derivatives of the dynamics are automatically included. Another backward sweep method implements this strategy in Alg. 10.

Algorithm 8 Forward pass with dynamics approximation and automatic differentiation

Input: $\varepsilon_{\text{DA}}, X, U, x_t, A, B, \mathcal{P}_f, l, \Phi$
 $k \leftarrow 0$
 $J^*, x_k^* \leftarrow 0, x_0$
while $k \leq N - 1$ **do**
 $\delta x_k^* \leftarrow x_k^* - x_k$
 $\delta u_k^* \leftarrow a_k + b_k \cdot \delta x_k^*$
 $u_k^* \leftarrow u_k + \delta u_k^*$
 Compute $R_{\varepsilon_{\text{DA}}, k}$
 if $\sqrt{\|\delta x_k^*\|_2^2 + \|\delta u_k^*\|_2^2} < R_{\varepsilon_{\text{DA}}, k}$ **then**
 $\mathcal{P}_{f,k} \leftarrow \mathcal{P}_{f,k}(\delta x_k^* + \delta x, \delta u_k^* + \delta u)$
 else
 $\mathcal{P}_{f,k} \leftarrow f(x_k^* + \delta x, u_k^* + \delta u)$
 end if
 $\mathcal{P}_{l,k} \leftarrow l(x_k^* + \delta x, u_k^* + \delta u)$
 $x_{k+1}^*, J^* \leftarrow \mathcal{P}_{f,k}, J^* + \mathcal{P}_{l,k}$
 $k \leftarrow k + 1$
end while
 $\mathcal{P}_\Phi \leftarrow \Phi(x_N^* + \delta x, x_t)$
 $J^* \leftarrow J^* + \mathcal{P}_\Phi$
Return: $J^*, X^*, U^*, \mathcal{P}_f, \mathcal{P}_l, \mathcal{P}_\Phi$

Algorithm 9 Backward sweep with automatic differentiation and Hessians

Input: $X, U, x_t, \mathcal{P}_f, \mathcal{P}_l, \mathcal{P}_\Phi$
Retrieve $V_{N,x}$ and $V_{N,xx}$ from \mathcal{P}_Φ
 $k \leftarrow N - 1$
while $k \geq 0$ **do**
 Retrieve $f_{k,x}, f_{k,u}, f_{k,xx}, f_{k,xu}, f_{k,uu}$ from $\mathcal{P}_{f,k}$
 Retrieve $l_{k,x}, l_{k,u}, l_{k,xx}, l_{k,xu}, l_{k,uu}$ from $\mathcal{P}_{l,k}$
 Compute $Q_{k,x}, Q_{k,u}, Q_{k,xx}, Q_{k,xu}, Q_{k,uu}$ with second order derivatives of f_k
 $a_k, b_k \leftarrow -Q_{k,uu}^{-1} \cdot Q_{k,u}^T, -Q_{k,uu}^{-1} \cdot Q_{k,xu}^T$
 Compute $V_{k,x}$ and $V_{k,xx}$
 $k \leftarrow k - 1$
end while
Return: A, B

Algorithm 10 Backward sweep with automatic differentiation and direct Q_k evaluation

Input: $X, U, x_t, \mathcal{P}_f, \mathcal{P}_l, \mathcal{P}_\Phi$
 $k \leftarrow N - 1$
 $\mathcal{P}_{V,k} \leftarrow \mathcal{P}_\Phi$
while $k \geq 0$ **do**
 $\mathcal{P}_{Q,k} \leftarrow \mathcal{P}_{l,k} + \mathcal{P}_{V,k+1}(\mathcal{P}_{f,k} - x_{k+1}, \mathbf{0})$
 Retrieve $Q_{k,x}, Q_{k,u}, Q_{k,xx}, Q_{k,xu}, Q_{k,uu}$ from $\mathcal{P}_{Q,k}$
 $a_k, b_k \leftarrow -Q_{k,uu}^{-1} \cdot Q_{k,u}^T, -Q_{k,uu}^{-1} \cdot Q_{k,xu}^T$
 $\mathcal{P}_{V,k} \leftarrow \mathcal{P}_{Q,k}(\delta x, a_k + b_k \cdot \delta x)$
 $k \leftarrow k - 1$
end while
Return: A, B

B. Fuel-optimal optimization

The energy-optimal problem is smooth and consists of a stage cost function of type: $l_E(\mathbf{x}, \mathbf{u}) = \frac{\mathbf{u}^T \cdot \mathbf{u}}{2}$. However, if \mathbf{u} is the thrust vector of a spacecraft, the stage cost to minimize to achieve minimum fuel is of type: $l_F(\mathbf{x}, \mathbf{u}) = \sqrt{\mathbf{u}^T \cdot \mathbf{u}}$, which implies the evaluation of the square root of the control. Yet, when $\mathbf{u} \approx \mathbf{0}$ the derivatives of l_F diverge since the square root is non-differentiable at $\mathbf{u} = \mathbf{0}$. Gradient-based optimization solvers, such as DDP, struggle and the DA framework does not apply anymore. Therefore, the authors present an alternative stage cost function l_H based on the pseudo-Huber loss function [19]:

$$l_H(\mathbf{x}, \mathbf{u}) = \sigma \cdot \left[\sqrt{\frac{\mathbf{u}^T \cdot \mathbf{u}}{\sigma^2} + 1} - 1 \right] \quad (12)$$

where σ is a tuning parameter. Note that:

$$l_H(\mathbf{x}, \mathbf{u}) \sim \begin{cases} \frac{\mathbf{u}^T \cdot \mathbf{u}}{2\sigma} = \frac{l_E(\mathbf{x}, \mathbf{u})}{\sigma}, & \text{if } \frac{\mathbf{u}^T \cdot \mathbf{u}}{\sigma^2} \ll 1 \\ \sqrt{\mathbf{u}^T \cdot \mathbf{u}} = l_F(\mathbf{x}, \mathbf{u}), & \text{if } \frac{\mathbf{u}^T \cdot \mathbf{u}}{\sigma^2} \gg 1 \end{cases} \quad (13)$$

Therefore, the singularity no longer exists. The strategy to converge to the fuel-optimal problem is to use an homotopy between l_E and l_H :

$$l(\mathbf{x}, \mathbf{u}) = \eta \cdot l_E(\mathbf{x}, \mathbf{u}) + (1 - \eta) \cdot l_H(\mathbf{x}, \mathbf{u}) \quad (14)$$

A first round of energy-optimal optimization is performed ($\eta = 1$). Then, the goal is to converge to $\eta \approx 0$ and $\sigma \approx 0$ so that: $l \sim l_F$.

C. Newton method acceleration

The goal of this part is to accelerate the run time of Alg. 5 using the same dynamics approximations method as in Section III.A.2 and methods for faster solving of symmetric block tri-diagonal systems. Indeed, solving of the system $\Delta^T \cdot \mathbf{z} = -\mathbf{d}$ of unknown \mathbf{z} to obtain δY^* comes down to solving the system: $\Delta \cdot \Delta^T \cdot \mathbf{z} = -\Delta \cdot \mathbf{d}$ of unknown \mathbf{z} . If $\tilde{\mathbf{g}}$ (respectively $\tilde{\mathbf{h}}$) is the vector of the active constraints of $\mathbf{g}(\mathbf{h})$, and $\tilde{\mathbb{I}}_{k, N_x}$ is \mathbb{I}_{N_x} , the identity of size $N_x \times N_x$, after

Algorithm 11 Modified Newton solver

Input: $\varepsilon_N, X_0, U_0, x_t, f, l, \Phi, g, g_t$
 Compute Y
 $d_{\max}, \gamma \leftarrow +\infty, 0.5$
while $d_{\max} > \varepsilon_N$ **do**
 $\mathcal{P}_\Gamma \leftarrow \Gamma(Y + \delta Y)$
 $d \leftarrow \overline{\mathcal{P}_\Gamma}$
 Compute Σ and Δ from \mathcal{P}_Γ
 $\Pi \leftarrow \text{BlockCholesky}(\Sigma)$
 $r \leftarrow +\infty$
 while $d_{\max} > \varepsilon_N \wedge r > \varepsilon_{CV}$ **do**
 $\delta Y^* \leftarrow -\Delta^T \cdot (\Pi^T \setminus (\Pi \setminus d))$
 $d_{\max}^*, \alpha \leftarrow +\infty, 1$
 while $d_{\max}^* > d_{\max}$ **do**
 $d^* \leftarrow \mathcal{P}_\Gamma(\alpha \cdot \delta Y^*)$
 $d_{\max}^*, \alpha \leftarrow \max |d^*|, \gamma \cdot \alpha$
 end while
 $Y, \mathcal{P}_\Gamma \leftarrow Y + \frac{\alpha}{\gamma} \cdot \delta Y^*, \mathcal{P}_\Gamma \left(\frac{\alpha}{\gamma} \cdot \delta Y^* + \delta Y \right)$
 $d \leftarrow d^*$
 $r, d_{\max} \leftarrow \log d_{\max}^* / \log d_{\max}, \max |d|$
 end while
end while
Return: X, U, d_{\max}

Table 1 Developed DDP methods and their names.

	Forward pass		
	Algorithm	Alg. 6	Alg. 8
	Alg. 7	Std	Dyn
Backward sweep	Alg. 9	Hess	HessDyn
	Alg. 10	Q	QDyn

Fig. 1 represents the implementation of the DADDy solver. This work proposes modifications to the forward pass, the backward sweep, and the Newton solver, which are highlighted in bold in the flow chart. Two forward pass algorithms and three backward sweep algorithms were presented in Section III.A. Thus, six different DDP solvers can be tested. They are listed and named in Table 1. Method Std, which stands for Standard, corresponds to an implementation of the ALTRO solver [13] and serves as state-of-the-art for next comparisons. The Newton solver used in DADDy is the one developed in Alg. 11.

IV. Applications

This section focuses on the validation of the DADDy solver and application to various test cases found in the literature. They include a double integrator problem and an Earth-Mars energy-optimal low-thrust transfer for validation [10], followed by the solving of fuel-optimal low-thrust transfers such as Earth to Mars [10], L_2 halo to L_1 halo [12, 14], L_2 near-rectilinear halo orbit (NRHO) to distant retrograde orbit (DRO) [14], Lyapunov L_1 to Lyapunov L_2 [12], DRO to

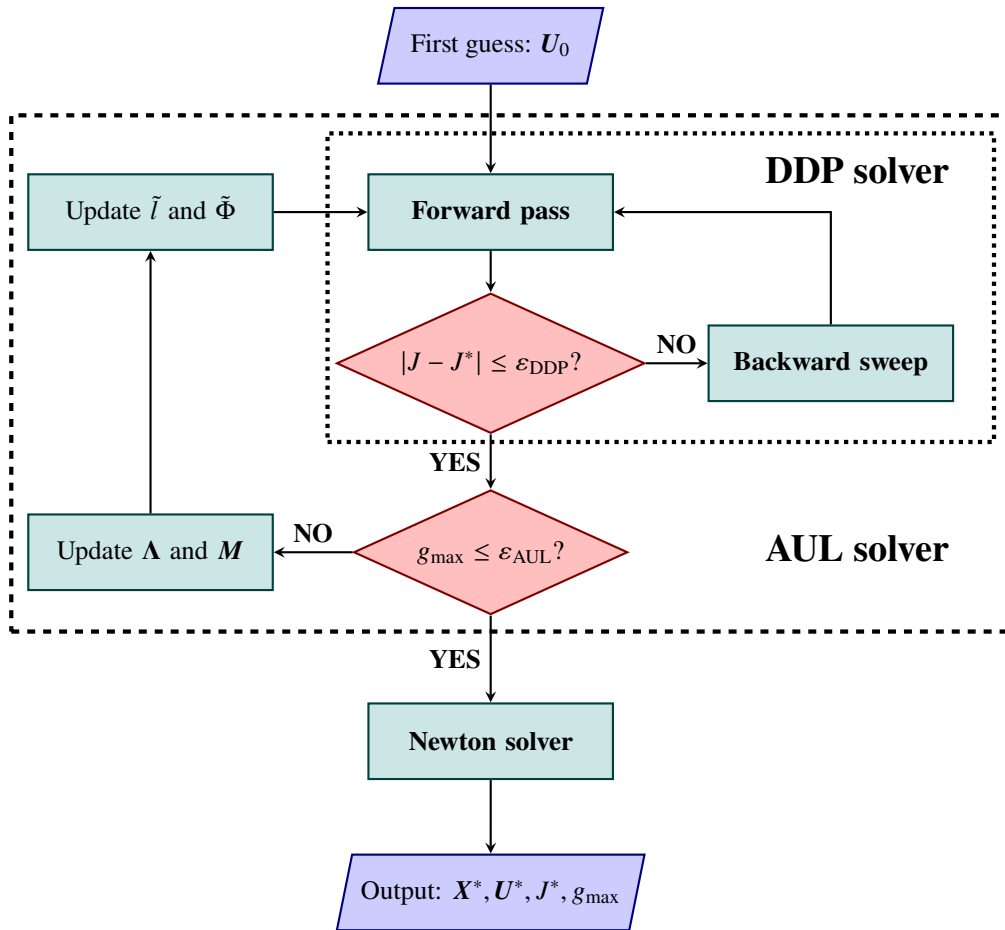


Fig. 1 Summary flow chart of the DADDy solver.

Table 2 Double integrator convergence data.

DDP method	Std	Hess	Q	Dyn	HessDyn	QDyn
Run time [ms (%Std)]	4.66 (–)	6.94 (149)	4.37 (93.7)	5.28 (113)	7.31 (157)	4.82 (103)
Cost function [-]	1.1273	1.1273	1.1273	1.1273	1.1273	1.1273

DRO [12], low Earth orbit (LEO) to LEO [22], medium Earth orbit (MEO) to MEO, geostationary transfer orbit (GTO) to geostationary orbit (GEO).

The solver was entirely developed in C++*, and uses the differential algebra core engine (DACE)† the polynomial computational engine, implemented by Dinamica SRL for ESA [23, 24]. All computations and run time analyses were performed on an Intel® Xeon® Gold 6126 CPU at 2.6 GHz.

A. Validation

1. DDP solvers validation

The DDP solvers developed for this work were validated against the unconstrained double integrator optimization problem from Lantoine and Russell [10]. The optimization problem is defined by:

$$\begin{cases} \mathbf{f}(\mathbf{x}, \mathbf{u}) &= [\mathbf{v}^T, \mathbf{u}^T]^T \\ l(\mathbf{x}, \mathbf{u}) &= \mathbf{u}^T \cdot \mathbf{u} \\ \Phi(\mathbf{x}, \mathbf{x}_t) &= (\mathbf{r} - \mathbf{r}_t)^T \cdot (\mathbf{r} - \mathbf{r}_t) \end{cases} \quad (17)$$

where $N_x = 6$, $N_u = 3$, $\mathbf{x} = [x, y, z, v^x, v^y, v^z]^T = [\mathbf{r}^T, \mathbf{v}^T]^T$, with \mathbf{r} the position of size $\frac{N_x}{2}$, and $\mathbf{v} = \dot{\mathbf{r}}$ the velocity. The number of stages is $N = 11$, and the initial conditions and target of the problem are $\mathbf{x}_0 = [1, 1, 1, 1, 1, 1]^T$ and $\mathbf{x}_t = [1, -1, 0, 0, 0, 0]^T$. This problem was solved by every DDP solver presented in Table 1, with as first guess \mathbf{U}_0 : a $N \cdot N_u$ vector with all components equal to 10^{-5} . They all return the same results, shown in Fig. 2, in a single iteration. Fig. 2a shows the states and Fig. 2b the controls. The results match the ones of Lantoine and Russell [10] and Table 2 provides additional information on the total cost and run time of each DDP method. All methods converged to the global optimum, which validates all DDP methods, but the run times are often higher for newly developed methods as they are up to 57% slower than Std.

*Library available at: <https://github.com/ThomasC1b/DADDy.git> [last accessed Sep 1, 2024].

†Library available at: <https://github.com/dace1ib/dace> [last accessed Sep 1, 2024].

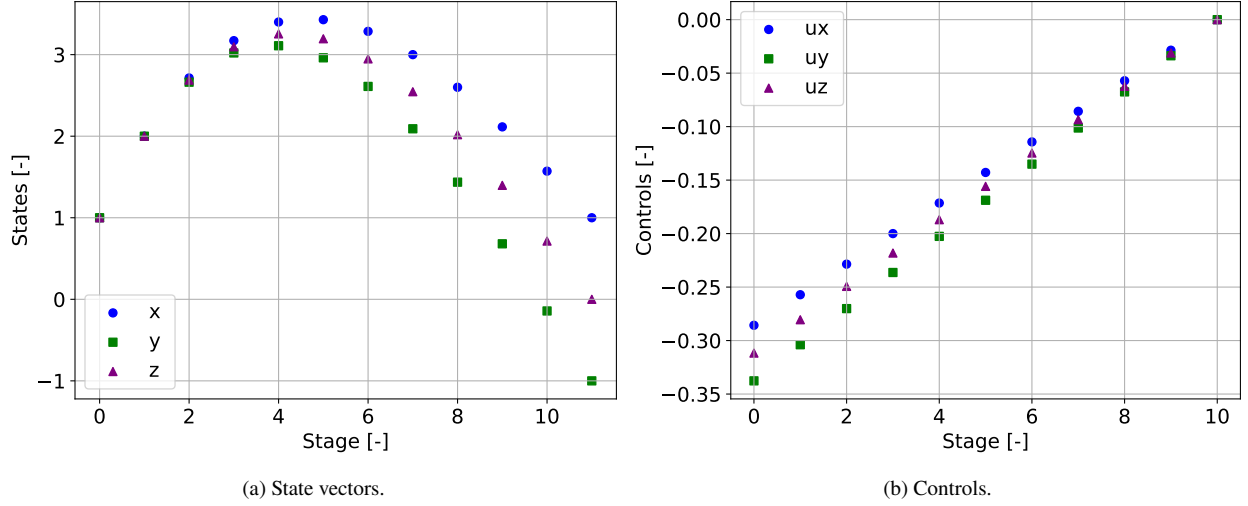


Fig. 2 Solution to the double integrator problem.

Table 3 Earth-Mars two-body problem transfer initial and target states.

Type	x [km]	y [km]	z [km]	\dot{x} [km/s]	\dot{y} [km/s]	\dot{z} [km/s]	m [kg]
Departure	-140 699 693	-51 614 428	980	9.774 596	-28.078 28	$4.337 725 \times 10^{-4}$	1000
Target	-172 682 023	176 959 469	7 948 912	-16.427 384	-14.860 506	$9.214 86 \times 10^{-2}$	-

2. AUL solver validation

The AUL solver was validated against an energy-optimal low-thrust Earth-Mars transfer optimization problem adapted from Lantoine and Russell [10]:

$$\left\{ \begin{array}{l}
 \mathbf{f}(\mathbf{x}, \mathbf{u}) = [\mathbf{v}^T, \dot{\mathbf{v}}^T, \dot{m}]^T \\
 \dot{\mathbf{v}} = -\frac{\mu}{\|\mathbf{r}\|_2^3} \mathbf{r} + \frac{\mathbf{u}}{m} \\
 \dot{m} = -\frac{\|\mathbf{u}\|_2}{g_0 \cdot Isp} \\
 l(\mathbf{x}, \mathbf{u}) = \frac{\mathbf{u}^T \cdot \mathbf{u}}{2} \\
 \Phi(\mathbf{x}, \mathbf{x}_t) = (\mathbf{r} - \mathbf{r}_t)^T \cdot (\mathbf{r} - \mathbf{r}_t) + (\mathbf{v} - \mathbf{v}_t)^T \cdot (\mathbf{v} - \mathbf{v}_t) \\
 \mathbf{g}_{ineq}(\mathbf{x}, \mathbf{u}) = [\mathbf{u}^T \cdot \mathbf{u} - u_{max}^2, m_{dry} - m]^T \\
 \mathbf{g}_{teq}(\mathbf{x}, \mathbf{x}_t) = [(\mathbf{r} - \mathbf{r}_t)^T, (\mathbf{v} - \mathbf{v}_t)^T]^T
 \end{array} \right. \quad (18)$$

where $N_x = 7$, $N_u = 3$, the state vector \mathbf{x} can be written: $[x, y, z, \dot{x}, \dot{y}, \dot{z}, m]$ or $[\mathbf{r}^T, \mathbf{v}^T, m]^T$, and m is the spacecraft mass. The number of stages is $N = 40$, the time-of-flight (ToF) is 348.79 d, the initial conditions and target are given in Table 3. Normalization units and various dynamics parameters are reported in Table 4. All mass parameters in this

Table 4 Sun-centered normalization units and dynamics parameters.

Type	Unit	Symbol	Value	Comment
Normalization units	Mass parameter [-]	μ	$1.327\,124\,400\,41 \times 10^{11}$	Sun's mass parameter
	Length [km]	LU	149 597 870.7	Astronomical unit of length
	Time [s]	TU	5 022 642.891	$(\text{LU}^3/\mu)^{1/2}$
	Velocity [km/s]	VU	29.784 691 83	LU/TU
Parameters	Standard gravity [m/s^2]	g_0	9.81	
	Specific impulse [s]	I_{sp}	2000	
	Spacecraft dry mass [kg]	m_{dry}	500	
	Maximum spacecraft thrust [N]	u_{max}	0.5	

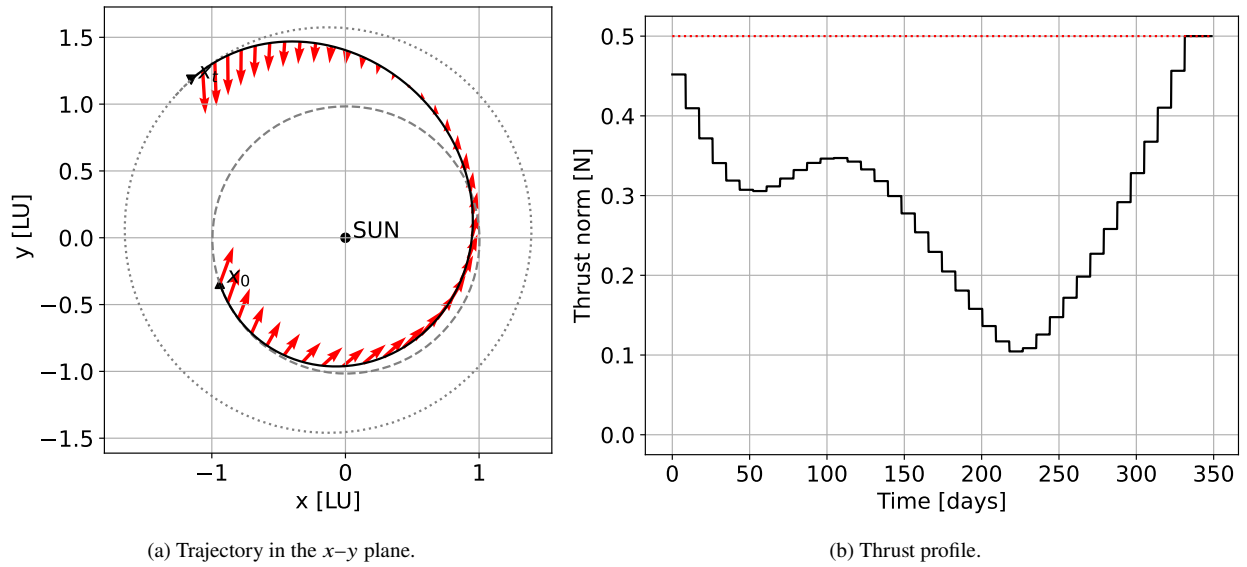


Fig. 3 Solution to the energy-optimal Earth-Mars transfer.

work were obtained from JPL DE431 ephemerides * [25]. The first guess U_0 is a $N \cdot N_u$ vector with all components equal to 1×10^{-6} N, and the various tolerance parameters are set to: $\varepsilon_{AUL} = \varepsilon_{DA} = 10^{-6}$, $\varepsilon_{DDP} = 10^{-4}$, and $\varepsilon_N = 10^{-10}$. Fig. 3 shows the solution to this optimization problem. Fig. 3a shows the trajectory from Earth to Mars, where the red arrows represent the thrust vectors. Fig. 3b represents the control norm, where the dotted red line is the control maximum magnitude u_{max} . Quantitative results are shown in Table 5. All methods converge towards the same trajectory and satisfy the constraints with an accuracy higher than ε_N , which validates the AUL solvers. Moreover, methods with dynamics Hessians converge in fewer DDP iterations, and run times are from 25% to 54% shorter for the newly developed methods. Comparing the methods implementing dynamics approximation with the rest, i.e., Std against Dyn, Hess against HessDyn, and Q against QDyn, shows the run time per iteration is smaller. This data highlights the acceleration provided by high-order Taylor polynomial use. The Newton solver is the same for all methods, and it

*Publicly available at: https://naif.jpl.nasa.gov/pub/naif/generic_kernels/pck/gm_de431.tpc [retrieved on Sep 1, 2024].

Table 5 Energy-optimal Earth-Mars transfer convergence data.

Data	Std	Hess	Q	Dyn	HessDyn	QDyn
g_{max} [-]	4×10^{-15}	5×10^{-15}	4×10^{-15}	3×10^{-15}	4×10^{-15}	3×10^{-15}
m_N [kg]	56.41	56.41	56.41	56.41	56.41	56.41
AUL iterations [-]	7	7	7	7	7	7
DDP iterations [- (%Std)]	47 (-)	28 (60)	39 (83)	47 (100)	28 (60)	42 (89)
AUL run time [s (%Std)]	4.8 (-)	2.9 (60)	3.6 (75)	3.3 (69)	2.2 (46)	3.1 (65)

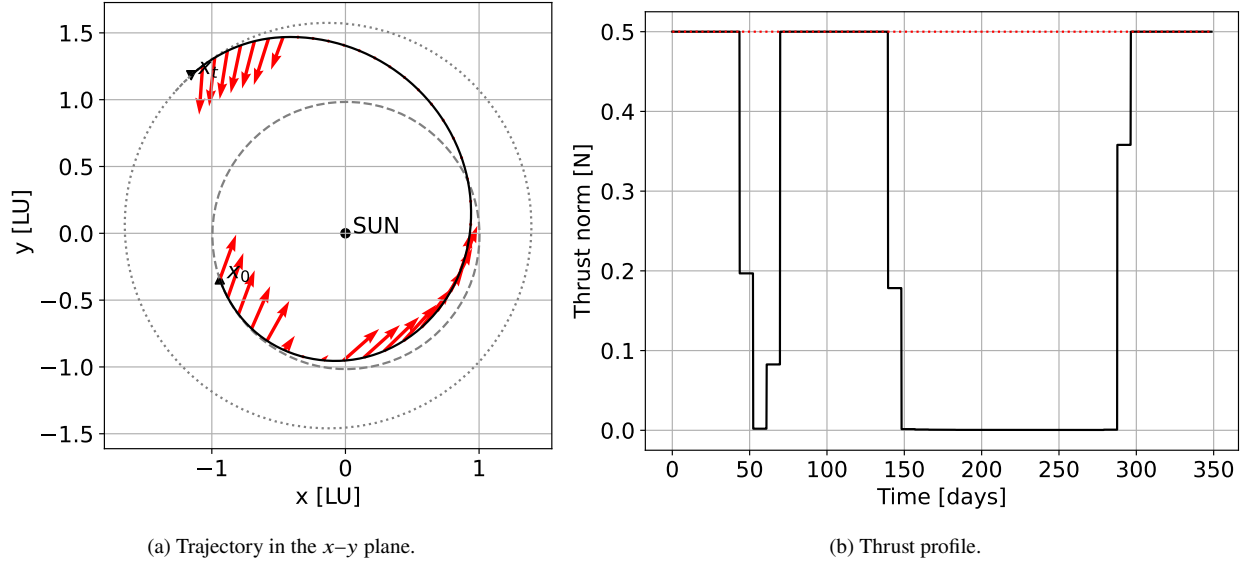


Fig. 4 Solution to the fuel optimal Earth-Mars transfer.

converged in the six cases in 0.5 s and 41 or 42 iterations, which validates the Newton solver.

3. Fuel-optimal solving

To validate the fuel-optimal solving method, the low-thrust Earth-Mars transfer optimization problem from Lantoine and Russell [10] is solved. This problem is the same as the one solved in Section IV.A.2, but where the stage cost l of Eq. (18) is replaced by the expression of Eq. (14). Fuel-optimal optimization is performed in four stages for (σ, η) : $(1, 10^{-2}) \rightarrow (0.5, 10^{-2}) \rightarrow (10^{-1}, 2 \times 10^{-3}) \rightarrow (10^{-3}, 10^{-3})$. Fig. 4 shows the solution to this problem, which visually matches the results of [10]. Fig. 4a shows the trajectory from Earth to Mars and Fig. 4b represents the control norm. The convergence results are reported in Table 6, where m_N is the fuel mass remaining after the transfer. All methods reach satisfactory constraints violation and converge to the same trajectory. The main difference is the run time, where the three methods with dynamics approximation are more than three times faster than Std. The Hess and Q methods also reduce the overall runtime. Yet, these gains vanish with dynamics approximation, i.e., for HessDyn and QDyn.

Table 6 Fuel-optimal Earth-Mars transfer convergence data.

Data	Std	Hess	Q	Dyn	HessDyn	QDyn
g_{max} [-]	1×10^{-11}	3×10^{-9}	5×10^{-11}	7×10^{-13}	3×10^{-11}	2×10^{-11}
m_N [kg]	103.32	103.22	102.78	103.44	103.26	103.38
Run time [s (%Std)]	27 (-)	18 (67)	16 (58)	8.2 (30)	8.4 (31)	8.5 (31)

Table 7 Earth-Moon CR3BP normalization units and parameters.

Unit	Symbol	Value	Comment
Mass parameter of M_1 [km^3/s^2]	GM_1	398 600	Earth's mass parameter GM_1
Mass parameter of M_2 [km^3/s^2]	GM_2	4902.80	Moon's mass parameter GM_2
Mass parameter [-]	μ	$1.215 06 \times 10^{-2}$	$GM_2/(GM_1 + GM_2)$
Length [km]	LU	384 399	Earth-Moon average distance
Time [s]	TU	375 189	$(\text{LU}^3/(GM_1 + GM_2))^{1/2}$
Velocity [km/s]	VU	1.024 55	LU/TU

B. Earth-Moon circular restricted three-body problem (CR3BP) transfers

The solver is now tested on trajectory optimization problems in the Earth-Moon CR3BP system [26, 27]. The dynamics take the following form:

$$\begin{cases} \mathbf{f}(\mathbf{x}, \mathbf{u}) &= [\dot{x}, \dot{y}, \dot{z}, \ddot{x}, \ddot{y}, \ddot{z}, \dot{m}]^T \\ \ddot{x} &= 2\dot{y} + \frac{\partial \Omega}{\partial x} + \frac{u^x}{m} \\ \ddot{y} &= -2\dot{x} + \frac{\partial \Omega}{\partial y} + \frac{u^y}{m} \\ \ddot{z} &= \frac{\partial \Omega}{\partial z} + \frac{u^z}{m} \\ \dot{m} &= -\frac{\|\mathbf{u}\|_2}{g_0 \cdot Isp} \end{cases} \quad (19)$$

where $N_x = 7$, $N_u = 3$, $\mathbf{x} = [x, y, z, \dot{x}, \dot{y}, \dot{z}, m]^T$, $\mathbf{u} = [u^x, u^y, u^z]$, and $\Omega = \frac{1}{2}(x^2 + y^2) + \frac{1 - \mu}{\sqrt{(x + \mu)^2 + y^2 + z^2}} + \frac{\mu}{\sqrt{(x + \mu - 1)^2 + y^2 + z^2}}$. The normalization units [28] are reported in Table 7. The stage cost is the one from Eq. (14), and the terminal cost, the path constraints and the terminal constraints are the same as in Eq. (18). Moreover, the spacecraft parameters are similar to those of Table 4 and the tolerances are the same. The solver was tested on four CR3BP test cases: (1) A transfer from a L_2 halo orbit [29, 30] to a L_1 halo used by Aziz et al. [12] and Boone and McMahon [14]. (2) A transfer from a L_2 NRHO [31] to a DRO [32] inspired by Boone and McMahon [14]. (3) A Lyapunov L_1 [32] to Lyapunov L_2 transfer from Aziz et al. [12]. (4) A DRO to DRO transfer from Aziz et al. [12]. The initial conditions, targets, ToFs and number of stages for each transfer are given in Table 8, the initial spacecraft mass, including dry mass, is 1000 kg and \mathbf{U}_0 is a $N \cdot N_u$ vector with all components equal to 1×10^{-6} N for all cases. The values for the Isp , g_0 , the maximum thrust magnitude, and the dry mass of the spacecraft are the same as in the

Table 8 Earth-Moon CR3BP transfers data.

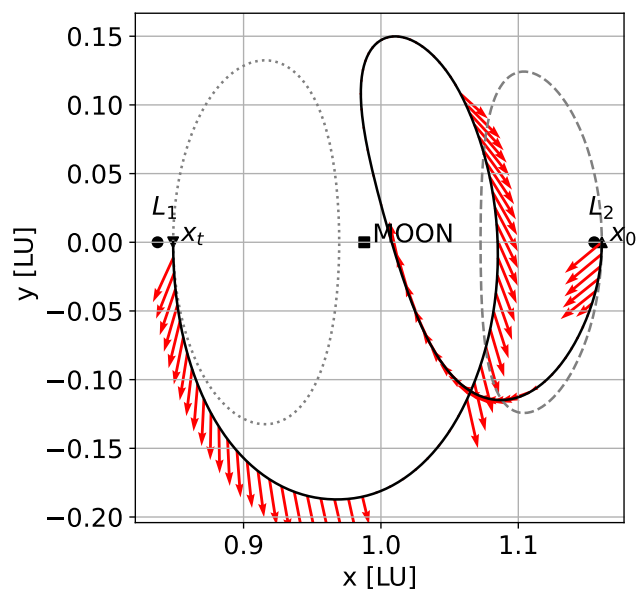
Transfer	ToF [d]	N	Type	x [LU]	y [LU]	z [LU]	\dot{x} [VU]	\dot{y} [VU]	\dot{z} [VU]
Halo L_2 to halo L_1	20	110	Initial	1.160 80	0	-0.122 70	0	-0.207 68	0
			Target	0.848 71	0	0.173 89	0	0.263 50	0
NRHO L_2 to DRO	21.2	150	Initial	1.021 97	0	-0.182 06	0	-0.103 14	0
			Target	0.983 37	0.259 21	0	0.351 34	-0.008 33	0
Lyapunov L_1 to Lyapunov L_2	12	300	Initial	0.855 99	0.124 37	0	0.094 85	0.044 11	0
			Target	1.095 98	0.115 26	0	0.037 47	0.126 74	0
DRO to DRO	17.5	100	Initial	1.171 36	0	0	0	-0.489 46	0
			Target	1.301 84	0	0	0	-0.642 18	0
DRO to DRO, 2 revs	33	300							
DRO to DRO, 3 revs	52.75	200							

Same as DRO to DRO

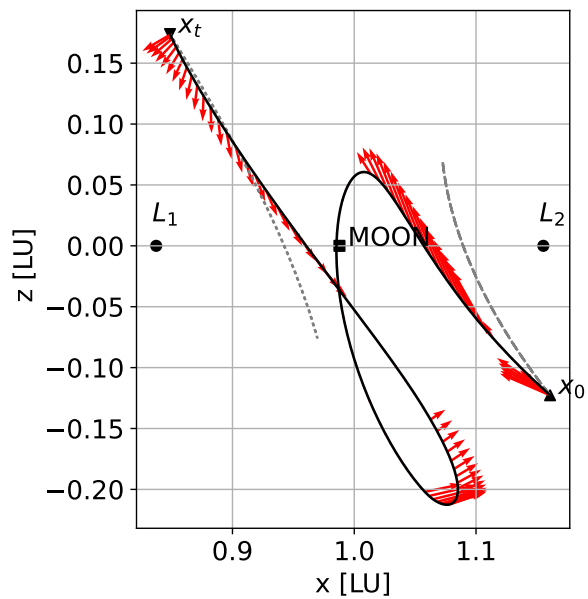
Earth-Mars transfer test case, reported in Table 4.

Fig. 5 shows the solutions to the halo L_2 to halo L_1 fuel-optimal transfers. Fig. 5a, Fig. 5b, and Fig. 5c show respectively the transfer in the x - y plane, in the x - z plane and its thrust profile, which is similar to Aziz et al. [12] and Boone and McMahon [14]. Fig. 6 shows the solution to the NRHO to DRO fuel-optimal transfer. Fig. 6a shows the trajectory in the x - y plane, while Fig. 6b shows the thrust profile. Fig. 7 shows the solution to the L_1 Lyapunov to L_2 Lyapunov fuel-optimal transfer. Fig. 7a shows the trajectory in the x - y plane, while Fig. 7b shows the thrust profile. Finally, Fig. 8 shows the solutions to the DRO to DRO fuel-optimal transfers, which correspond to the results of Aziz et al. [12]. Fig. 8a, Fig. 8c, and Fig. 8e respectively show the trajectories for the single, two, or three revolution test case. While Fig. 8b, Fig. 8d, and Fig. 8f show the thrust profiles in the same order.

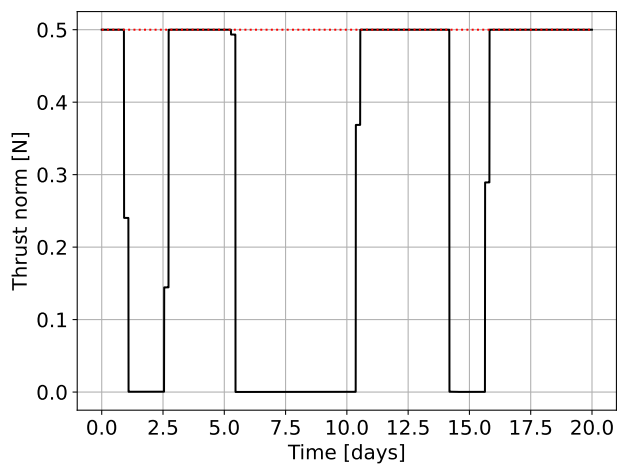
As expected, all resulting solutions correspond to bang-bang control laws, as expected for fuel-optimal transfers. The convergence data are given in Table 9, where the mention did not converge (DNC) is given when the algorithm did not terminate. Results show that, upon convergence, all six methods reach highly similar results. However, the methods implementing dynamics Hessians seem highly unstable and converge only in less than 60% of test cases. On the other side, the Dyn method always brings similar results as Std with 33% to 94% shorter run times. In the case of the DRO-to-DRO transfer, the extra revolutions provide smaller fuel consumption using the Dyn method, similarly as Aziz et al. [12].



(a) Trajectory in the x - y plane.



(b) Trajectory in the x - z plane.



(c) Thrust profile.

Fig. 5 Solution to the halo L_2 to halo L_1 fuel-optimal transfer.

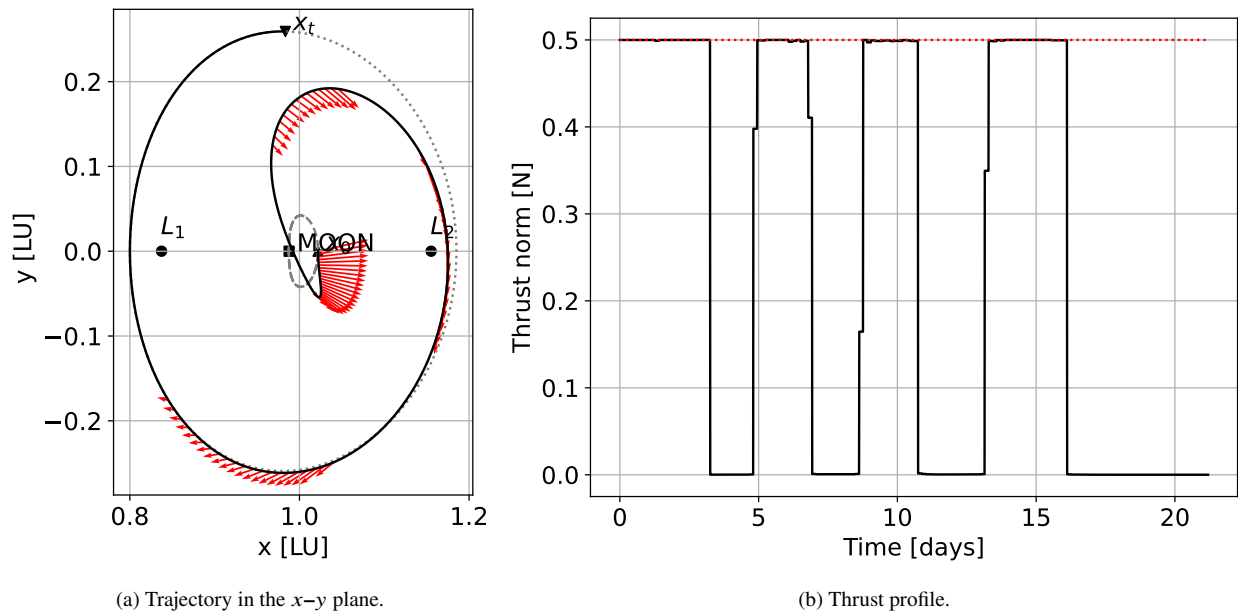


Fig. 6 Solution to the L_2 NRHO to DRO fuel-optimal transfer.

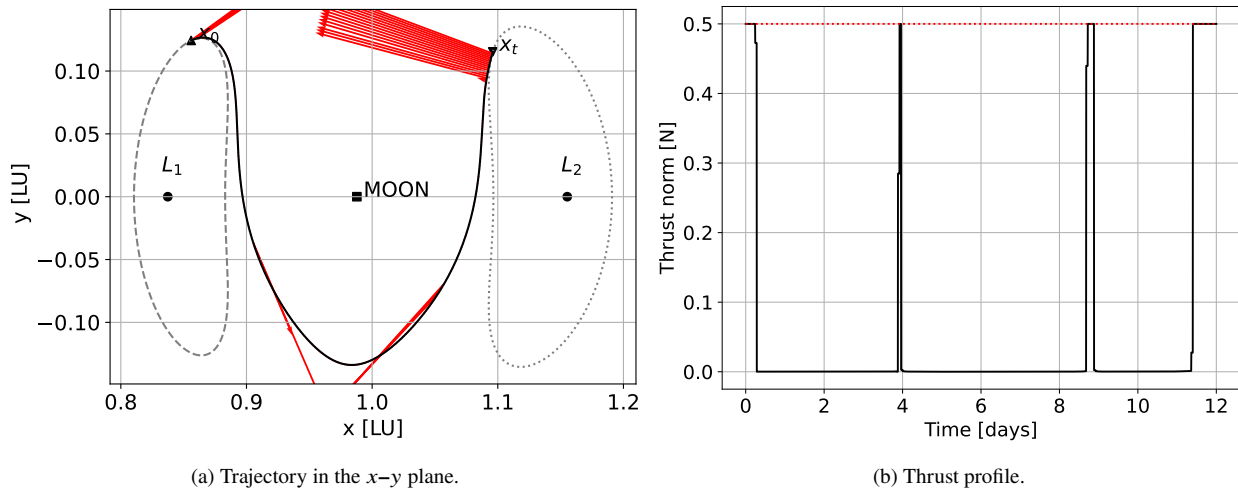
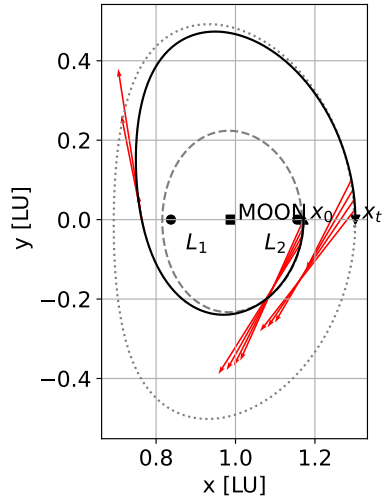
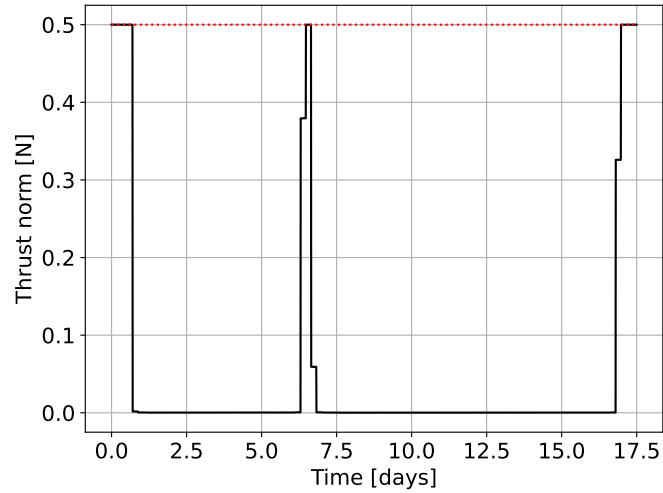


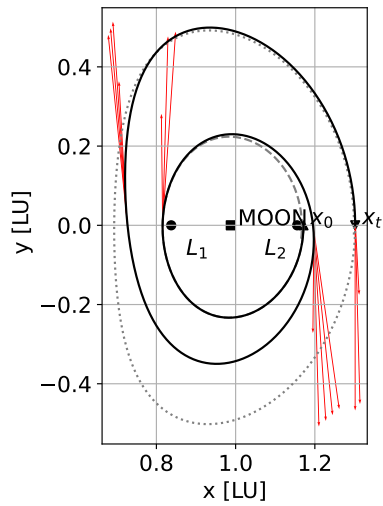
Fig. 7 Solution to the L_1 Lyapunov to L_2 Lyapunov fuel-optimal transfer.



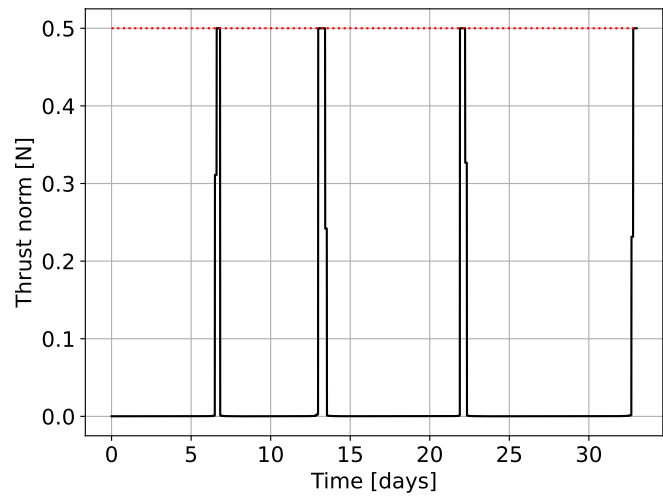
(a) Single-revolution trajectory in the x - y plane.



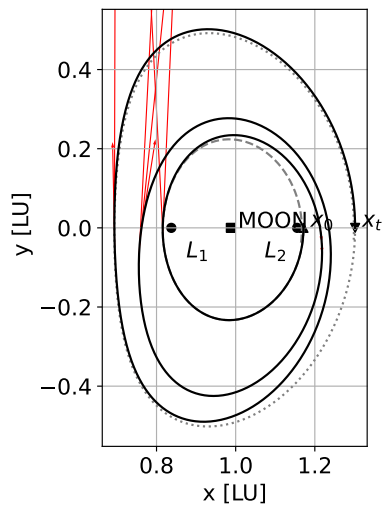
(b) Thrust profile of the single-revolution transfer.



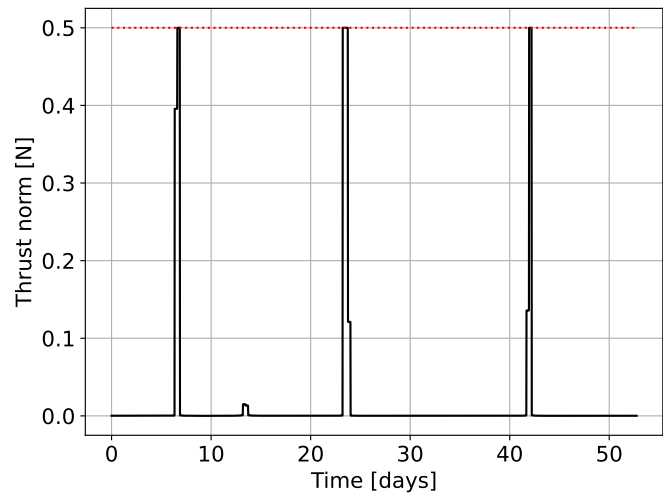
(c) Two-revolutions trajectory in the x - y plane.



(d) Thrust profile of the two-revolutions transfer.



(e) Three-revolutions trajectory in the x - y plane.



(f) Thrust profile of the three-revolutions transfer.

Fig. 8 Solutions to the DRO to DRO fuel-optimal transfers in a single revolution (top), two revolutions (middle) or three revolutions (bottom).

Table 9 Convergence data for fuel-optimal CR3BP transfers.

Transfer	Data	Std	Hess	Q	Dyn	HessDyn	QDyn
Halo L_2 to halo L_1	g_{max} [-]	2×10^{-8}	3×10^{-9}	1×10^{-9}	7×10^{-10}	7×10^{-9}	7×10^{-11}
	m_N [kg]	473.31	473.83	473.78	473.93	473.80	473.77
	Run time [s (%Std)]	110 (-)	57 (53)	57 (53)	31 (29)	28 (26)	30 (28)
NRHO L_2 to DRO	g_{max} [-]	8×10^{-15}			7×10^{-11}		
	m_N [kg]	477.34			477.39		
	Run time [s (%Std)]	410 (-)		DNC	50 (12)		DNC
Lyapunov L_1 to Lyapunov L_2	g_{max} [-]	1×10^{-10}			8×10^{-10}		
	m_N [kg]	497.43			497.49		
	Run time [s (%Std)]	830 (-)			140 (17)		
DRO to DRO	g_{max} [-]	8×10^{-11}	1×10^{-12}	5×10^{-13}	9×10^{-11}	1×10^{-10}	1×10^{-10}
	m_N [kg]	496.05	496.32	496.32	496.32	496.30	496.32
	Run time [s (%Std)]	200 (-)	38 (19)	53 (26)	13 (6.3)	19 (9.1)	17 (8.4)
DRO to DRO, 2 revs	g_{max} [-]	1×10^{-10}	2×10^{-10}	1×10^{-9}	1×10^{-10}	3×10^{-10}	
	m_N [kg]	496.77	491.53	491.44	496.77	491.56	DNC
	Run time [s (%Std)]	190 (-)	480 (260)	550 (290)	83 (44)	242 (130)	
DRO to DRO, 3 revs	g_{max} [-]	5×10^{-11}	1×10^{-10}	10×10^{-10}	5×10^{-11}	1×10^{-10}	1×10^{-10}
	m_N [kg]	496.86	495.56	495.55	496.86	495.56	495.55
	Run time [s (%Std)]	79 (-)	180 (230)	500 (630)	61 (77)	150 (190)	200 (250)

C. Earth-centered transfers

Earth-centered two-body [33] optimization problems were also tackled. The Gauss equations of motion are written in the equinoctial form from Di Carlo et al. [34]:

$$\left\{ \begin{array}{l}
 \mathbf{f}(\mathbf{x}, \mathbf{u}) = [\dot{a}, \dot{p}, \dot{q}, \dot{r}, \dot{s}, \dot{\mathcal{L}}, \dot{m}]^T \\
 \dot{a} = \frac{2}{\mathcal{B}} \sqrt{\frac{a^3}{\mu}} [(q \sin \mathcal{L} - p \cos \mathcal{L}) \cdot u^R + \Psi] \\
 \dot{p} = \mathcal{B} \sqrt{\frac{a}{\mu}} \left[-\cos \mathcal{L} \cdot u^R + \left(\frac{p + \sin \mathcal{L}}{\Psi} + \sin \mathcal{L} \right) \cdot u^L - q \frac{r \cos \mathcal{L} - s \sin \mathcal{L}}{\Psi} \cdot u^N \right] \\
 \dot{q} = \mathcal{B} \sqrt{\frac{a}{\mu}} \left[\sin \mathcal{L} \cdot u^R + \left(\frac{q + \cos \mathcal{L}}{\Psi} + \cos \mathcal{L} \right) \cdot u^L + p \frac{r \cos \mathcal{L} - s \sin \mathcal{L}}{\Psi} \cdot u^N \right] \\
 \dot{r} = \frac{\mathcal{B}}{2} \sqrt{\frac{a}{\mu}} (1 + r^2 + s^2) \frac{\sin \mathcal{L}}{\Psi} \cdot u^N \\
 \dot{s} = \frac{\mathcal{B}}{2} \sqrt{\frac{a}{\mu}} (1 + r^2 + s^2) \frac{\cos \mathcal{L}}{\Psi} \cdot u^N \\
 \dot{\mathcal{L}} = \sqrt{\frac{\mu}{a}} \frac{\Psi^2}{\mathcal{B}^3} - \sqrt{\frac{a^3}{\mu}} \frac{\mathcal{B}}{\Psi} (r \cos \mathcal{L} - s \sin \mathcal{L}) \cdot u^N \\
 \dot{m} = -\frac{\|\mathbf{u}\|_2}{g_0 \cdot Isp} \\
 \Phi(\mathbf{x}, \mathbf{x}_t) = (\mathbf{r} - \mathbf{r}_t)^T \cdot (\mathbf{r} - \mathbf{r}_t) \\
 \mathbf{g}_{teq}(\mathbf{x}, \mathbf{x}_t) = \mathbf{r} - \mathbf{r}_t
 \end{array} \right. \quad (20)$$

Table 10 Earth-centered normalization units and parameters.

Unit	Symbol	Value	Comment
Mass parameter [km ³ /s ²]	μ	398 600	Earth's mass parameter
Time [s]	TU	86 400	Mean solar day
Length [km]	LU	42 241	$[\mu \cdot (\text{TU}/(2\pi))^2]^{1/3}$
Velocity [km/s]	VU	0.488 90	LU/TU

where $N_x = 7$, $N_u = 3$, $\mathcal{B} = \sqrt{1 - p^2 - q^2}$, and $\Psi = 1 + p \sin \mathcal{L} + q \cos \mathcal{L}$, and where $\mathbf{x} = [a, p, q, r, s, \mathcal{L}, m] = [\mathbf{r}^T, \mathcal{L}, m]^T$ are the equinoctial coordinates:

$$\left\{ \begin{array}{l} a \\ p = e \sin (\Omega + \omega) \\ q = e \cos (\Omega + \omega) \\ r = \tan \frac{i}{2} \sin \Omega \\ s = \tan \frac{i}{2} \cos \Omega \\ L = \Omega + \omega + \nu \end{array} \right. \quad (21)$$

and $\mathbf{u} = [u^R, u^T, u^N]$ is the thrust vector in the radial-tangential-normal (RTN) reference frame. The mean longitude \mathcal{L} is neglected in the terminal cost and constraints. In other words, the position on the final orbit is not considered important. The stage cost is the one from Eq. (14), and the path constraints are from Eq. (18). The normalization units are reported in Table 10, the spacecraft parameters are similar as those of Table 4, and the tolerances are the same. Three test cases of the Earth-centered two-body problem will be tackled: (1) A transfer from a LEO to another LEO inspired by [22] (2) A transfer from a MEO to another MEO with a -35 deg change in Ω (3) A transfer from a GTO at perigee altitude 400 km to a GEO. The initial conditions, targets, ToFs and number of stages for each test case are given in Table 11. The initial spacecraft mass is set to 1000 kg, and the first guess is a $N \cdot N_u$ vector with all components equal to 1×10^{-6} N in all cases. The values for the Isp , g_0 , the maximum thrust magnitude, and the dry mass of the spacecraft are the same as in the Earth-Mars transfer test case, reported in Table 4.

Fig. 9 shows the solution to the LEO to LEO fuel-optimal transfer. Fig. 9a shows the evolution of the Keplerians and Fig. 9b shows the thrust profile. Similarly for Fig. 10, Fig. 10a, and Fig. 10b in the same order for the MEO to MEO fuel-optimal transfer, and with Fig. 11, Fig. 11a, and Fig. 11b for the GTO to GEO fuel-optimal transfer. The solutions are also bang-bang controls, the convergence data are given in Table 12.

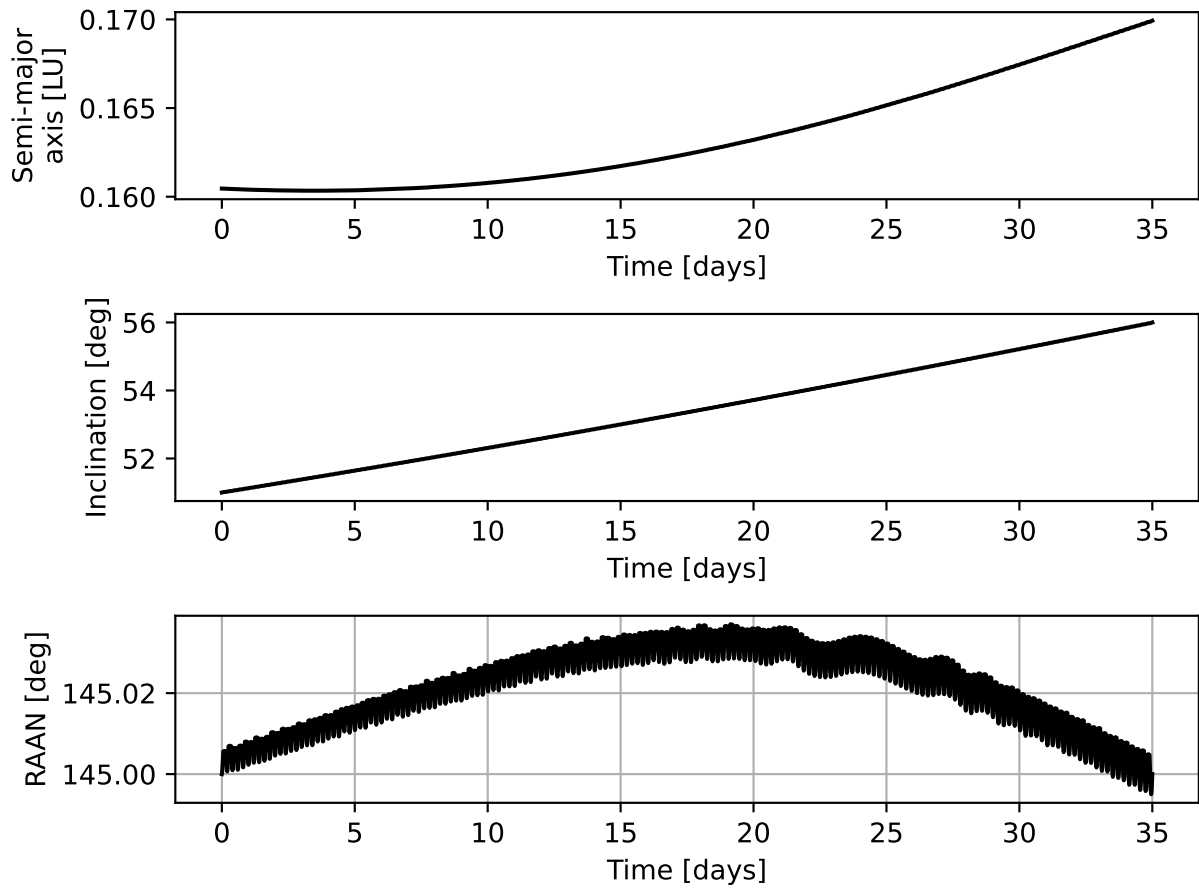
When they converge, methods implementing dynamic Hessians exhibit significantly faster convergence, thanks to the

Table 11 Earth-centered two-body problem transfers data.

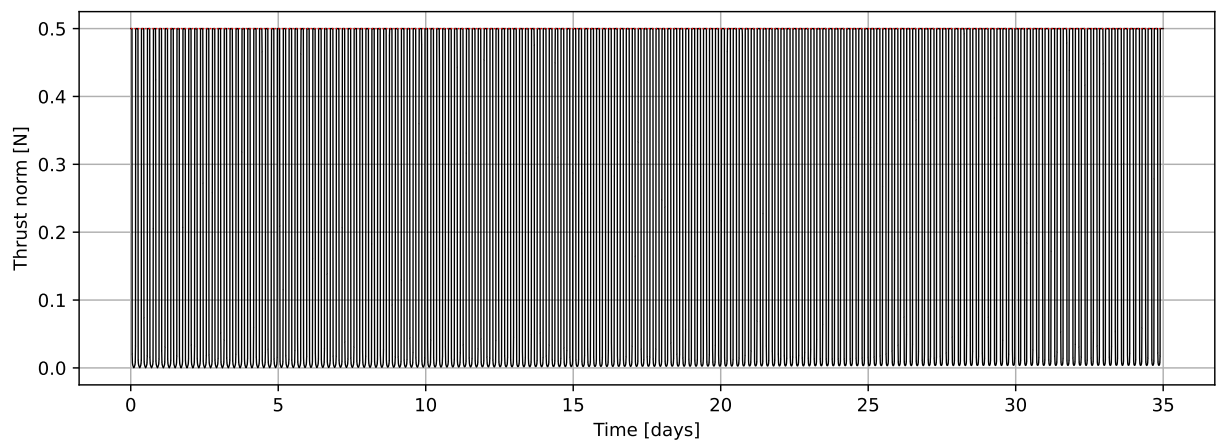
Transfer	ToF [d]	N	Type	a [km]	e [-]	i [deg]	Ω [deg]	ω [deg]	ν [deg]
LEO to LEO	35	5000	Initial	6778.0	0	51	145	–	0
			Target	7178.0	0	56	145	–	0
MEO to MEO	55	2500	Initial	34 378	0	60	180	–	0
			Target	34 378	0	60	155	–	0
GTO to GEO	95	10 000	Initial	24 480	0.723 116	0	–	0	0
			Target	42 181	0	0	–	–	0

Table 12 Convergence data for fuel-optimal Earth-centered two-body problem transfers.

Transfer	Data	Std	Hess	Q	Dyn	HessDyn	QDyn
LEO to LEO	g_{max} [-]	2×10^{-8}	4×10^{-10}	6×10^{-9}	3×10^{-8}	2×10^{-10}	2×10^{-8}
	m_N [kg]	459.50	458.66	455.47	459.83	458.13	456.88
	DDP iterations [- (%Std)]	6140 (-)	1977 (32.2)	1333 (21.7)	9580 (156)	5493 (89.5)	5019 (81.7)
	Run time [h (%Std)]	74 (-)	22 (29)	17 (22)	40 (54)	20 (26)	22 (29)
MEO to MEO	g_{max} [-]	5×10^{-12}	1×10^{-11}	6×10^{-12}	2×10^{-8}	6×10^{-12}	
	m_N [kg]	420.61	419.29	418.9	420.23	419.43	DNC
	DDP iterations [- (%Std)]	2242 (-)	845 (37.7)	1505 (67.1)	3183 (142)	1823 (81.3)	
	Run time [h (%Std)]	17 (-)	4.6 (27)	5.9 (35)	7.0 (41)	2.8 (16)	
GTO to GEO	g_{max} [-]				2×10^{-10}		
	m_N [kg]		DNC		410.48		DNC
	DDP iterations [- (%Std)]				3512 (-)		
	Run time [h (%Std)]				84 (-)		

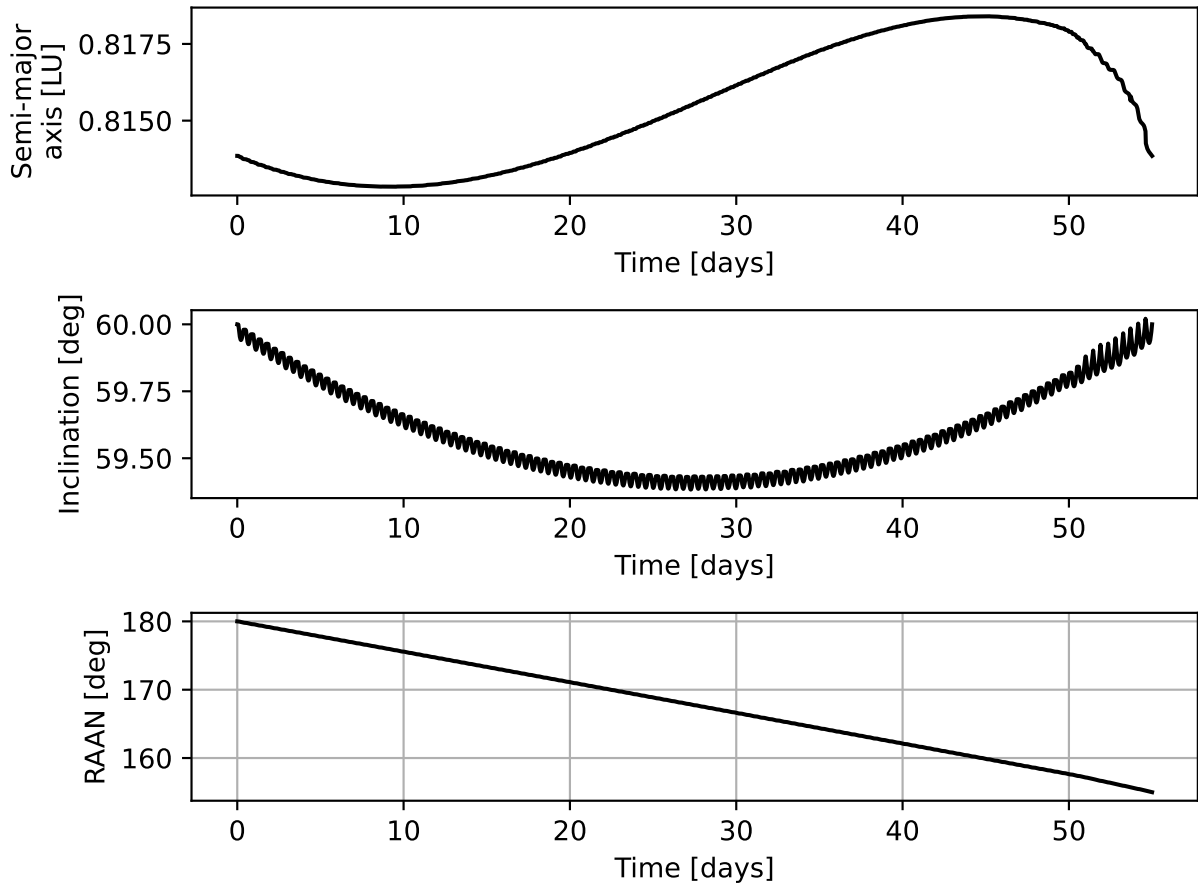


(a) Evolution of the Keplerians.

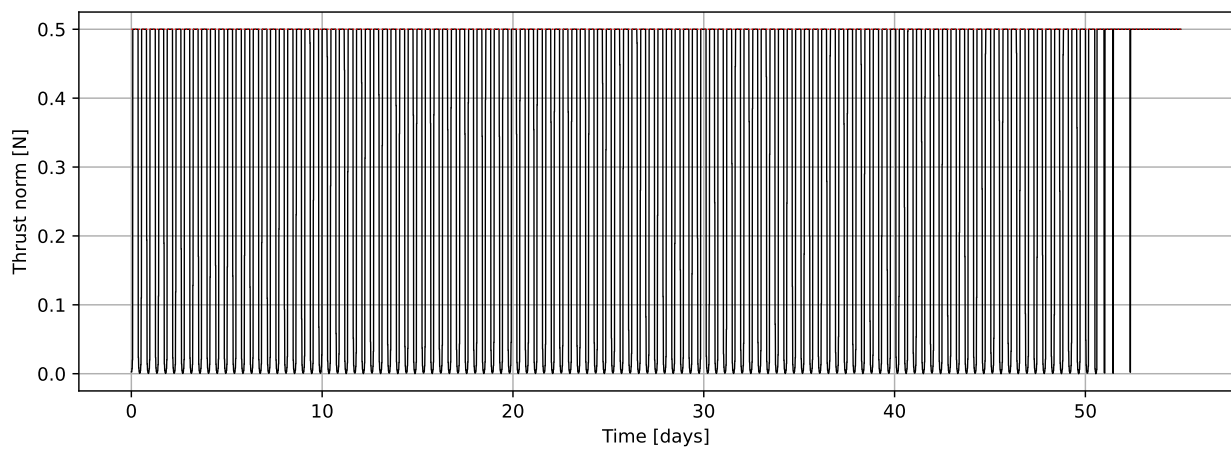


(b) Thrust profile.

Fig. 9 Solution to the LEO to LEO fuel-optimal transfer.

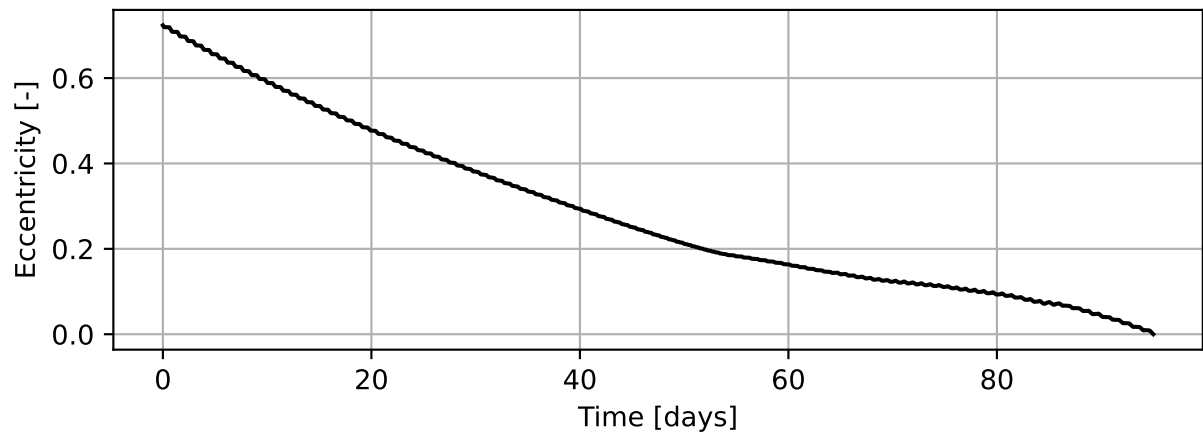
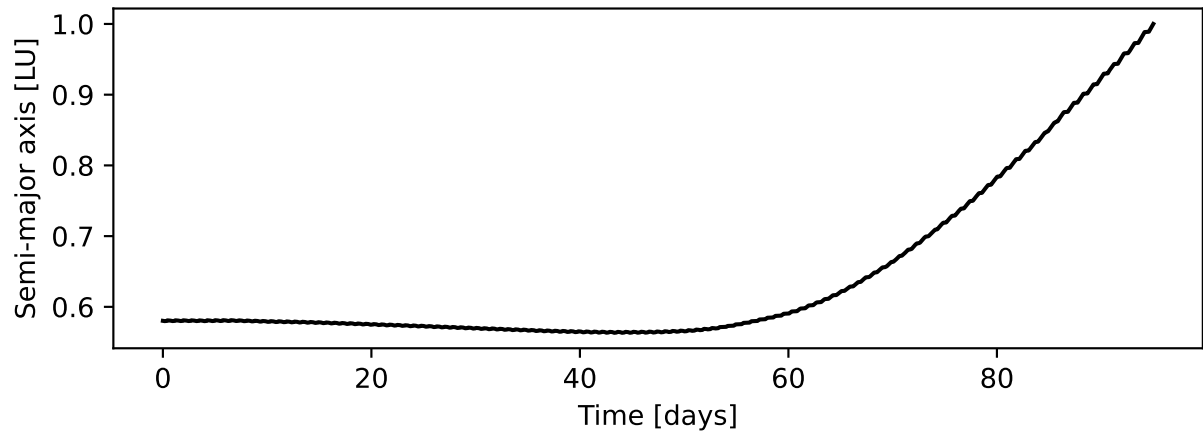


(a) Evolution of the Keplerians.

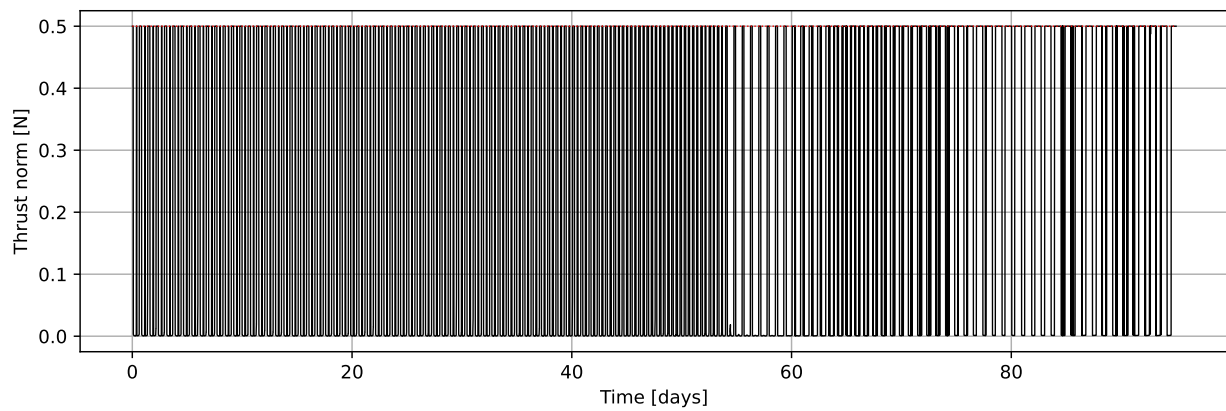


(b) Thrust profile.

Fig. 10 Solution to the MEO to MEO fuel-optimal transfer.



(a) Evolution of the Keplerians.



(b) Thrust profile.

Fig. 11 Solution to the GTO to GEO fuel-optimal transfer.

reduced number of iterations. Furthermore, the linearity of the dynamics, compared to the more complex CR3BP, means the accelerations provided by the Dyn methods are smaller. In the challenging GTO to GEO test case, most methods struggled to converge due to long ToFs. Note that in all three cases, the run times are prohibitively long. These performances can be explained by the fact that these problems require numerous switches and that the dynamics are implemented without any form of regularization, such as the Sundman transform [35], to improve convergence. However, these test cases represent a good stress test for the DADDy solver. Averaged analytical methods are a fast and adapted alternative to tackle similar optimization problems [22, 34].

V. Conclusions

This work proposed accelerated approaches for constrained differential dynamic programming (DDP) by using high-order Taylor expansions for both automatic differentiation and nonlinear dynamics approximation, without needing an initial feasible trajectory. The proposed framework enables efficient fuel-optimal trajectory optimization using pseudo-Huber loss function, with an enhanced solution polishing phase.

The Dyn method, i.e., with dynamics approximation and state-of-the-art backward sweep, is the most stable of the novel DDP method, with similar results as the literature. Moreover, it runs 33% to 94% faster than Std, the state-of-the-art method, without drawbacks. In addition, the differential algebra (DA) framework keeps the user from deriving and implementing the gradients by hand. Thus, the Dyn method is more satisfactory than state-of-the-art DDP. On the other hand, methods implementing Hessians of the dynamics have shown they can improve convergence speed at the cost of higher instability. It may explain why these Hessians are often neglected in certain solvers [6, 30]. Indeed, they represent extra computational efforts. For numerous-revolutions, i.e., Earth-centered, low-thrust transfers, the differential algebra-based differential dynamic programming (DADDy) solver's run time are impractical and cannot be used in operations or embedded space systems. The DADDy solver performs well in a wide range of trajectory optimization problems at low run times with satisfactory constraint violations. It opens the possibility of using this solver for embedded space systems.

Funding Sources

This work was funded by SaCLaB (grant number 2022-CIF-R-1), a research group of ISAE-SUPAERO.

References

- [1] Zheng, Y., Ouyang, Z., Li, C., Liu, J., and Zou, Y., "China's Lunar Exploration Program: Present and future," *Planetary and Space Science*, Vol. 56, No. 7, 2008, pp. 881–886. <https://doi.org/https://doi.org/10.1016/j.pss.2008.01.002>.
- [2] Smith, M., Craig, D., Herrmann, N., Mahoney, E., Krezel, J., McIntyre, N., and Goodliff, K., "The Artemis Program:

- An Overview of NASA's Activities to Return Humans to the Moon," *2020 IEEE Aerospace Conference*, 2020, pp. 1–10. <https://doi.org/10.1109/AERO47225.2020.9172323>.
- [3] Caleb, T., Armellin, R., and Lizy-Destrez, S., "Fast Gradient Evaluation and Mapping Method for Bi-Impulsive Transfers Within Periodic Orbits," *Journal of Guidance, Control, and Dynamics*, Vol. 0, No. 0, 2024, pp. 1–9. <https://doi.org/10.2514/1.G008038>, URL <https://arc.aiaa.org/doi/abs/10.2514/1.G008038>.
- [4] Riedel, J., Eldred, D., Kennedy, B., Kubitscheck, D., Vaughan, A., Werner, R., Bhaskaran, S., and Synnott, S., "AutoNav Mark3: Engineering the Next Generation of Autonomous Onboard Navigation and Guidance," *AIAA Guidance, Navigation, and Control Conference and Exhibit*, American Institute of Aeronautics and Astronautics, 2006. <https://doi.org/10.2514/6.2006-6708>.
- [5] Boone, S., and McMahon, J., "Orbital Guidance Using Higher-Order State Transition Tensors," *Journal of Guidance, Control, and Dynamics*, Vol. 44, No. 3, 2021, pp. 493–504. <https://doi.org/10.2514/1.g005493>.
- [6] Mayne, D., "A Second-order Gradient Method for Determining Optimal Trajectories of Non-linear Discrete-time Systems," *International Journal of Control*, Vol. 3, No. 1, 1966, pp. 85–95. <https://doi.org/10.1080/00207176608921369>, URL <https://doi.org/10.1080/00207176608921369>.
- [7] Rayman, M. D., Fraschetti, T. C., Raymond, C. A., and Russell, C. T., "Dawn: a mission in development for exploration of main belt asteroids Vesta and Ceres," *Acta Astronautica*, Vol. 58, No. 11, 2006, pp. 605–616. <https://doi.org/10.1016/j.actaastro.2006.01.014>.
- [8] Oh, D. Y., Collins, S. M., Goebel, D. M., Hart, B., Lantoine, G., Snyder, S., Whiffen, G. J., Elkins-Tanton, L. T., Lord, P. W., Pirkel, Z., and Rotlisburger, L., "Development of the Psyche mission for NASA's discovery program," *35th International Electric Propulsion Conference*, 2017. URL <https://api.semanticscholar.org/CorpusID:31454933>.
- [9] Lantoine, G., and Russell, R. P., "A Hybrid Differential Dynamic Programming Algorithm for Constrained Optimal Control Problems. Part 1: Theory," *Journal of Optimization Theory and Applications*, Vol. 154, No. 2, 2012, pp. 382–417. <https://doi.org/10.1007/s10957-012-0039-0>, URL <https://doi.org/10.1007/s10957-012-0039-0>.
- [10] Lantoine, G., and Russell, R. P., "A Hybrid Differential Dynamic Programming Algorithm for Constrained Optimal Control Problems. Part 2: Application," *Journal of Optimization Theory and Applications*, Vol. 154, No. 2, 2012, pp. 418–442. <https://doi.org/10.1007/s10957-012-0038-1>, URL <https://doi.org/10.1007/s10957-012-0038-1>.
- [11] Ozaki, N., Campagnola, S., Funase, R., and Yam, C. H., "Stochastic Differential Dynamic Programming with Unscented Transform for Low-Thrust Trajectory Design," *Journal of Guidance, Control, and Dynamics*, Vol. 41, No. 2, 2018, pp. 377–387. <https://doi.org/10.2514/1.G002367>, URL <https://doi.org/10.2514/1.G002367>.
- [12] Aziz, J. D., Scheeres, D. J., and Lantoine, G., "Hybrid Differential Dynamic Programming in the Circular Restricted Three-Body Problem," *Journal of Guidance, Control, and Dynamics*, Vol. 42, No. 5, 2019, pp. 963–975. <https://doi.org/10.2514/1.G003617>, URL <https://doi.org/10.2514/1.G003617>.

- [13] Howell, T. A., Jackson, B. E., and Manchester, Z., "ALTRO: A Fast Solver for Constrained Trajectory Optimization," *2019 IEEE/RSJ International Conference on Intelligent Robots and Systems (IROS)*, 2019, pp. 1–6. <https://doi.org/10.1109/IROS40897.2019.8967788>, URL <https://doi.org/10.1109/IROS40897.2019.8967788>.
- [14] Boone, S., and McMahon, J., "Rapid Local Trajectory Optimization in Cislunar Space," *AIAA/AAS Astrodynamics Specialist Conference*, 2022, pp. 1–20.
- [15] Berz, M., *Modern Map Methods in Particle Beam Physics*, Elsevier, 1999, Chap. 2. [https://doi.org/10.1016/s1076-5670\(08\)70227-1](https://doi.org/10.1016/s1076-5670(08)70227-1).
- [16] Armellin, R., Di Lizia, P., Bernelli-Zazzera, F., and Berz, M., "Asteroid close encounters characterization using differential algebra: the case of Apophis," *Celestial Mechanics and Dynamical Astronomy*, Vol. 107, No. 4, 2010, pp. 451–470. <https://doi.org/10.1007/s10569-010-9283-5>.
- [17] Berz, M., "High-order computation and normal form analysis of repetitive systems," *AIP Conference Proceedings*, 1992, pp. 1–36. <https://doi.org/10.1063/1.41975>.
- [18] Wittig, A., Di Lizia, P., Armellin, R., Makino, K., Bernelli-Zazzera, F., and Berz, M., "Propagation of large uncertainty sets in orbital dynamics by automatic domain splitting," *Celestial Mechanics and Dynamical Astronomy*, Vol. 122, No. 3, 2015, pp. 239–261. <https://doi.org/10.1007/s10569-015-9618-3>.
- [19] Barani, F., Savadi, A., and Sadoghi Yazdi, H., "A distributed learning based on robust diffusion SGD over adaptive networks with noisy output data," *Journal of Parallel and Distributed Computing*, Vol. 190, 2024, p. 104883. <https://doi.org/https://doi.org/10.1016/j.jpdc.2024.104883>, URL <https://www.sciencedirect.com/science/article/pii/S0743731524000479>.
- [20] Cholesky, A.-L., "Sur la résolution numérique des systèmes d'équations linéaires," Tech. rep., 1910.
- [21] Cao, T., Hall, J., and van de Geijn, R., "Parallel Cholesky factorization of a block tridiagonal matrix," *Proceedings. International Conference on Parallel Processing Workshop*, 2002, pp. 327–335. <https://doi.org/10.1109/ICPPW.2002.1039748>.
- [22] Di Carlo, M., and Vasile, M., "Analytical solutions for low-thrust orbit transfers," *Celestial Mechanics and Dynamical Astronomy*, Vol. 133, No. 7, 2021. <https://doi.org/10.1007/s10569-021-10033-9>, URL <https://doi.org/10.1007/s10569-021-10033-9>.
- [23] Rasotto, M., Morselli, A., Wittig, A., Massari, M., Di Lizia, P., Armellin, R., Yabar Valles, C., and Urbina Ortega, C., "Differential algebra space toolbox for nonlinear uncertainty propagation in space dynamics," *6th International Conference on Astrodynamics Tools and Techniques (ICATT)*, edited by G. uropean Space Operations Centre (ESOC), Darmstadt, 2016, pp. 1–11.
- [24] Massari, M., Di Lizia, P., Cavenago, F., and Wittig, A., "Differential Algebra software library with automatic code generation for space embedded applications," *2018 AIAA Information Systems-AIAA Infotech @ Aerospace*, American Institute of Aeronautics and Astronautics, 2018, pp. 1–13. <https://doi.org/10.2514/6.2018-0398>.

- [25] Folkner, W., Williams, J., Boggs, D., Park, R., and Kuchynka, P., “The Planetary and Lunar Ephemerides DE430 and DE431,” Tech. Rep. 42-196, Jet Propulsion Laboratory, California Institute of Technology, 2014.
- [26] Poincaré, H., *Les Méthodes Nouvelles de la Mécanique Céleste*, Gauthier-Villars, Paris, France, 1892.
- [27] Szebehely, V., *Theory of Orbits*, Academic Press, 1967. <https://doi.org/10.1016/B978-0-12-395732-0.50007-6>.
- [28] Jorba, A., and Masdemont, J., “Dynamics in the center manifold of the collinear points of the restricted three body problem,” *Physica D: Nonlinear Phenomena*, Vol. 132, No. 1, 1999, pp. 189–213. [https://doi.org/https://doi.org/10.1016/S0167-2789\(99\)00042-1](https://doi.org/https://doi.org/10.1016/S0167-2789(99)00042-1).
- [29] Farquhar, R. W., “The Control and Use of Libration-Point Satellites,” Tech. rep., National Aeronautics and Space Administration (NASA), 1970. Number NASA TR R-346.
- [30] Howell, K., “Three-dimensional, periodic, ‘halo’ orbits,” *Celestial Mechanics*, Vol. 32, No. 1, 1984, pp. 53–71. <https://doi.org/10.1007/bf01358403>.
- [31] Zimovan Spreen, E. M., Howell, K. C., and Davis, D. C., “Near rectilinear halo orbits and nearby higher-period dynamical structures: orbital stability and resonance properties,” *Celestial Mechanics and Dynamical Astronomy*, Vol. 132, No. 5, 2020, pp. 1–25. <https://doi.org/10.1007/s10569-020-09968-2>.
- [32] Hénon, M., “Numerical exploration of the restricted problem, V,” *Astronomy and Astrophysics*, Vol. 1, 1969, pp. 223–238.
- [33] Vallado, D. A., and McClain, W. D., *Fundamentals of Astrodynamics and Applications*, Hawthorne (CA) : Microcosm Press, 2007.
- [34] Di Carlo, M., Graça Marto, S. d., and Vasile, M., “Extended analytical formulae for the perturbed Keplerian motion under low-thrust acceleration and orbital perturbations,” *Celestial Mechanics and Dynamical Astronomy*, Vol. 133, No. 3, 2021. <https://doi.org/10.1007/s10569-021-10007-x>, URL <https://doi.org/10.1007/s10569-021-10007-x>.
- [35] Aziz, J. D., Parker, J. S., Scheeres, D. J., and Englander, J. A., “Low-Thrust Many-Revolution Trajectory Optimization via Differential Dynamic Programming and a Sundman Transformation,” *The Journal of the Astronautical Sciences*, Vol. 65, No. 2, 2018, pp. 205–228. <https://doi.org/10.1007/s40295-017-0122-8>.